WILEY

Online Proofing System

1. Corrections should be marked with the Adobe Annotation & Comment Tools below:

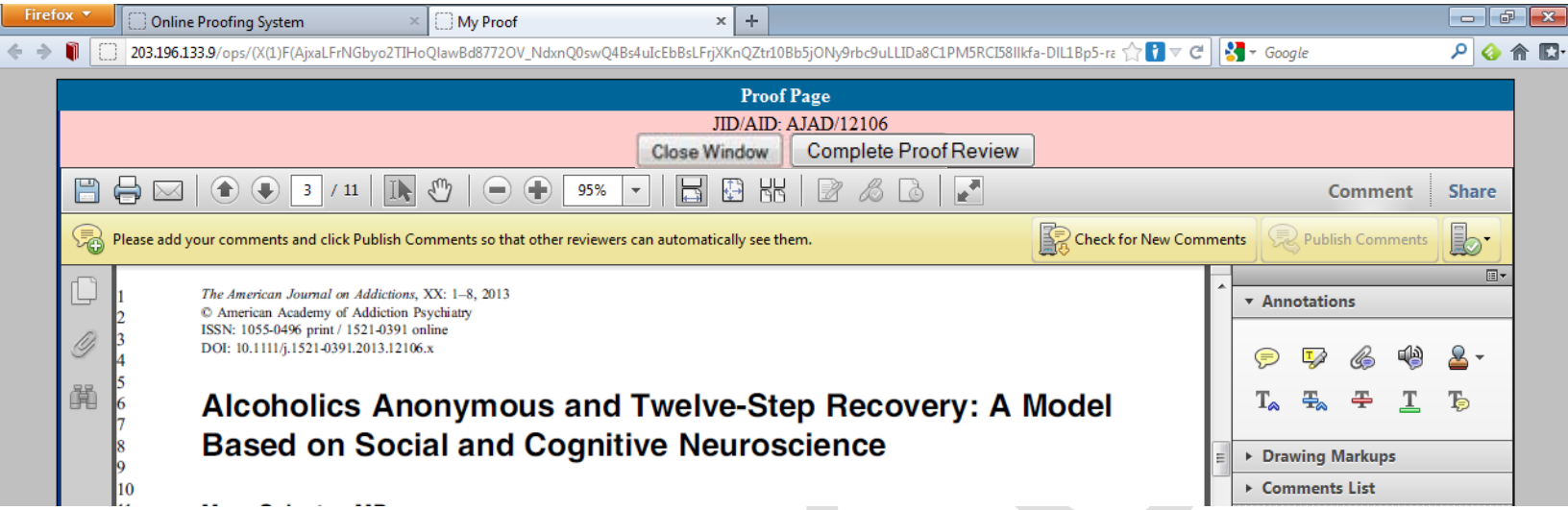

2. To save your proof corrections, click the 'Publish Comments' button. Publishing your comments saves the marked up version of your proof to a centralized location in Wiley's Online Proofing System. Corrections don't have to be marked in one sitting – you can publish corrections and log back in at a later time to add more.

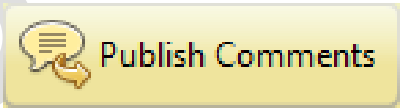

3. When your proof review is complete we recommend you download a copy of your annotated proof for reference in any future correspondence concerning the article before publication. You can do this by clicking on the icon to the right of the 'Publish Comments' button and selecting 'Save as Archive Copy…'.

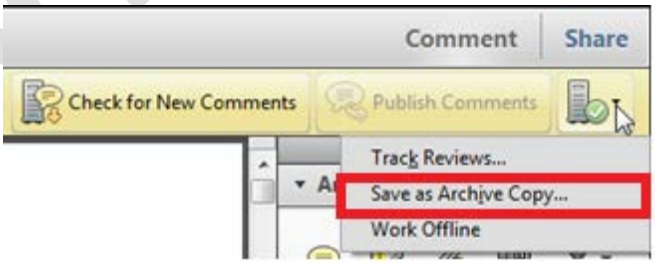

4. When your proof review is complete and you are ready to send corrections to the publisher click the 'Complete Proof Review' button that appears above the proof in your web browser window. Do not click the 'Complete Proof Review' button without replying to any author queries found on the last page of your proof. Incomplete proof reviews will cause a delay in publication. **Note: Once you click 'Complete Proof Review' you will not be able to mark any further comments or corrections**.

Firefox, Chrome, Safari Users

If your PDF article proof opens in any PDF viewer other than Adobe Reader or Adobe Acrobat, you will not be able to mark corrections and query responses, nor save them. To mark and save corrections, please follow these instructions to disable the built-in browser PDF viewers in Firefox, Chrome, and Safari so the PDF article proof opens in Adobe within a Firefox or Chrome browser window.

How to disable the built-in PDF viewer and use Adobe PDF viewer

If you use Firefox, Chrome, or Safari they have a built-in PDF viewer that hides essential OPS features needed for viewing/editing the PDF proofs. In order to override the built-in or native PDF viewer, please follow the instructions below.

FIREFOX

To switch from the built-in PDF viewer to Adobe PDF viewer Firefox:

1. At the top of the Firefox window, click on the Firefox button and then select Options (if you have an older version of Firefox, Options may be found by clicking the Tools button at the top of the window).
2. Select the Applications panel.
3. Find **Portable Document Format (PDF)** in the **Content Type** list and click on it to select it.
4. Click on the drop-down arrow in the **Action** column for the above entry and select **Use Adobe Acrobat (in Firefox).**

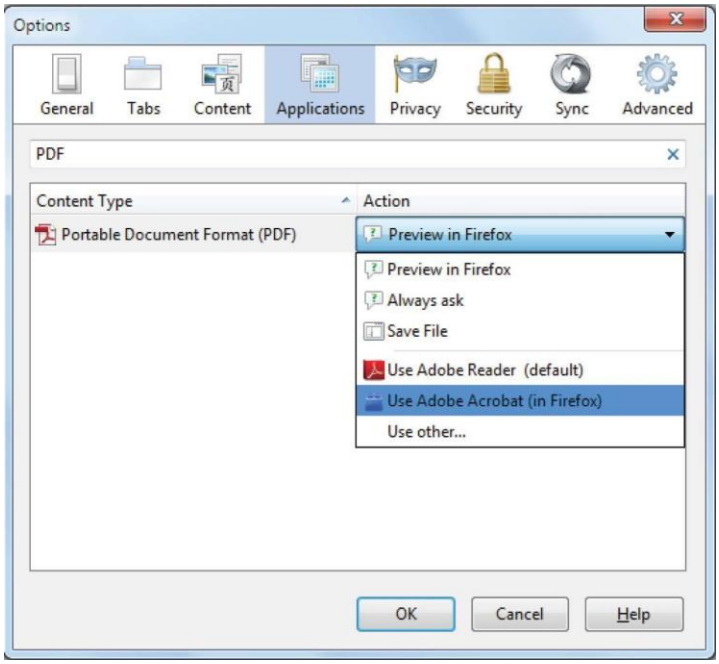

CHROME

To switch from the built-in PDF viewer to Adobe PDF viewer Chrome:

1. Open Chrome and type “chrome:plugins” in the URL bar in the browser.

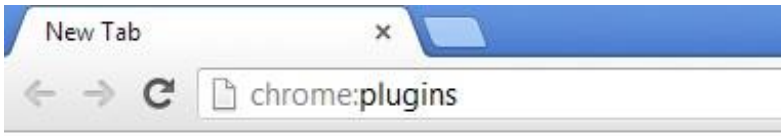

2. Scroll down and find ‘Chrome PDF viewer’.

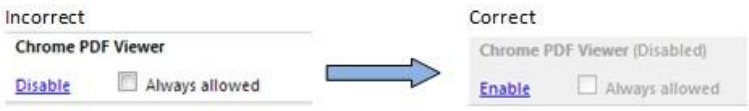

3. Click the ‘Disable’ link to prevent PDFs from opening in Chrome’s built-in PDF viewer.
4. Close and restart the web browser.
5. Now you can choose to download or open PDFs with Adobe on your PC. And if you ever change your mind, the option will be in the same place with an "Enable" link to bring it back.

Safari

To switch from the built-in PDF viewer to Adobe PDF viewer Chrome:

1. In the Finder, select a PDF, and choose File > Get Info.

2. Click the arrow next to Open With to expose the product menu.

3. Choose either Adobe Acrobat or Adobe Reader from the application menu.

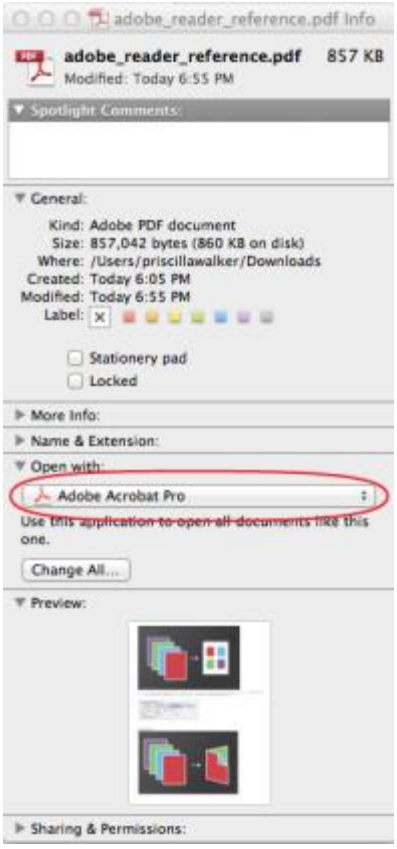

4. Click the Change All button.

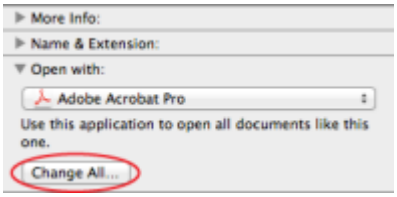

5. When asked if you want to change all similar documents, click Continue.

For more information About Enabling Adobe Acrobat or Reader in Safari please visit: http://helpx.adobe.com/acrobat/using/display-pdf-browser-acrobat-xi.html

USING e-ANNOTATION TOOLS FOR ELECTRONIC PROOF CORRECTION

Required software to e-Annotate PDFs: Adobe Acrobat Professional or Adobe Reader (version 8.0 or above). (Note that this document uses screenshots from Adobe Reader X)
The latest version of Acrobat Reader can be downloaded for free at: http://get.adobe.com/reader/

Once you have Acrobat Reader open on your computer, click on the Comment tab at the right of the toolbar:

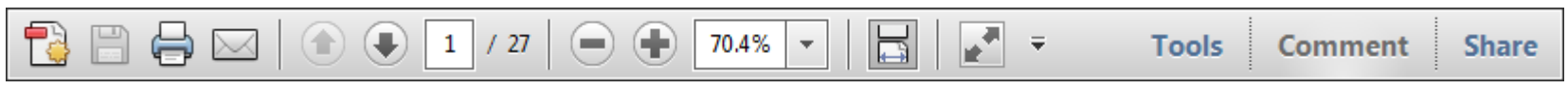

This will open up a panel down the right side of the document. The majority of tools you will use for annotating your proof will be in the Annotations section, pictured opposite. We've picked out some of these tools below:

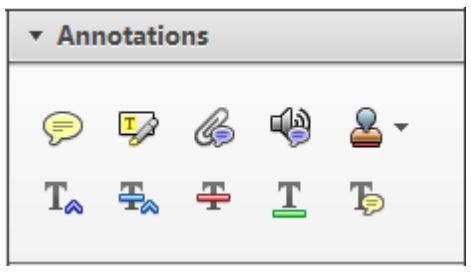

1. Replace (Ins) Tool – for replacing text.

Strikes a line through text and opens up a text box where replacement text can be entered.

How to use it

- Highlight a word or sentence.
- Click on the Replace (Ins) icon in the Annotations section.
- Type the replacement text into the blue box that appears.

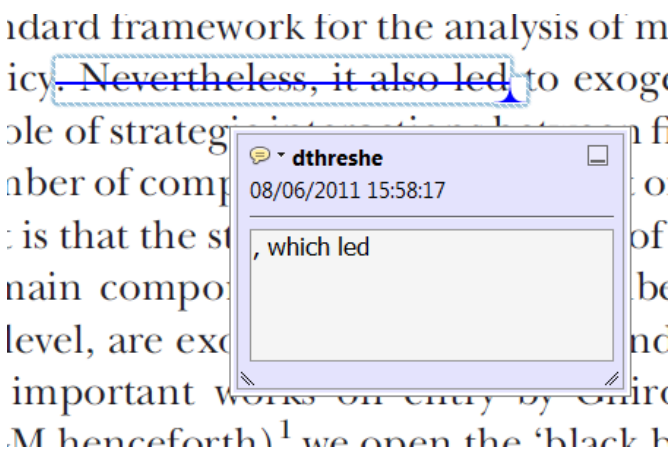

2. Strikethrough (Del) Tool – for deleting text.

Strikes a red line through text that is to be deleted.

How to use it

- Highlight a word or sentence.
- Click on the Strikethrough (Del) icon in the Annotations section.

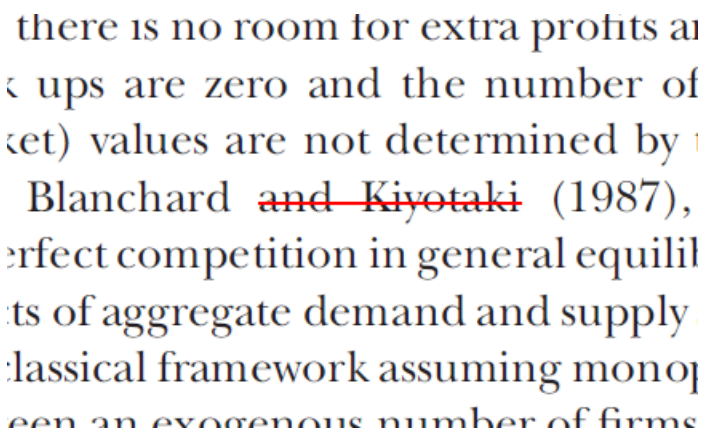

3. Add note to text Tool – for highlighting a section to be changed to bold or italic.

Highlights text in yellow and opens up a text box where comments can be entered.

How to use it

- Highlight the relevant section of text.
- Click on the Add note to text icon in the Annotations section.
- Type instruction on what should be changed regarding the text into the yellow box that appears.

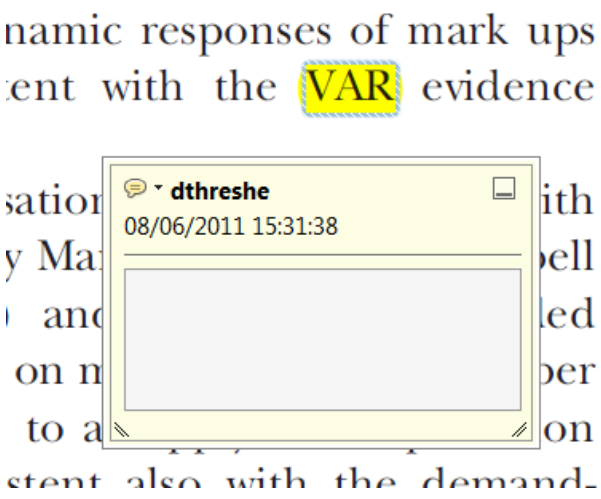

4. Add sticky note Tool – for making notes at specific points in the text.

Marks a point in the proof where a comment needs to be highlighted.

How to use it

- Click on the Add sticky note icon in the Annotations section.
- Click at the point in the proof where the comment should be inserted.
- Type the comment into the yellow box that appears.

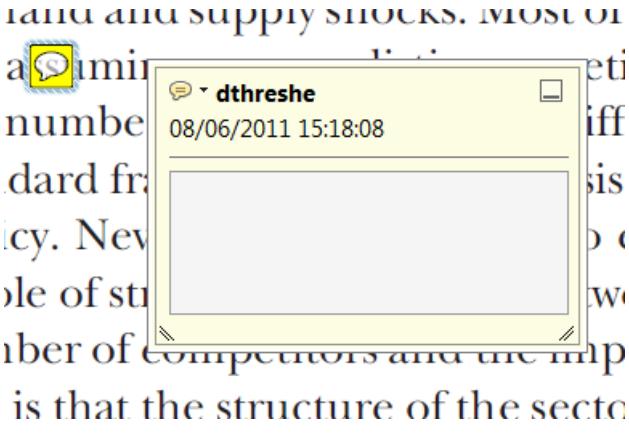

5. Attach File Tool – for inserting large amounts of text or replacement figures.

Inserts an icon linking to the attached file in the appropriate pace in the text.

How to use it

- Click on the Attach File icon in the Annotations section.
- Click on the proof to where you'd like the attached file to be linked.
- Select the file to be attached from your computer or network.
- Select the colour and type of icon that will appear in the proof. Click OK.

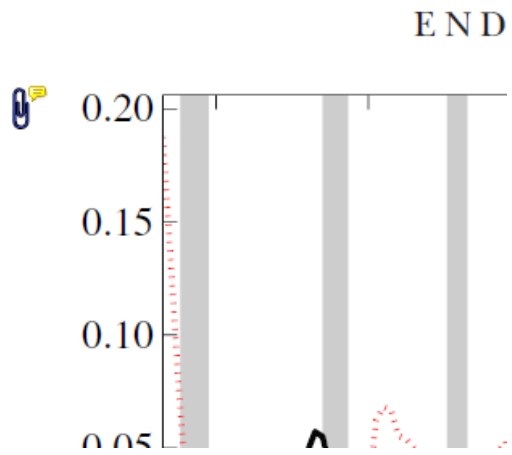

6. Add stamp Tool – for approving a proof if no corrections are required.

Inserts a selected stamp onto an appropriate place in the proof.

How to use it

- Click on the Add stamp icon in the Annotations section.
- Select the stamp you want to use. (The Approved stamp is usually available directly in the menu that appears).
- Click on the proof where you'd like the stamp to appear. (Where a proof is to be approved as it is, this would normally be on the first page).

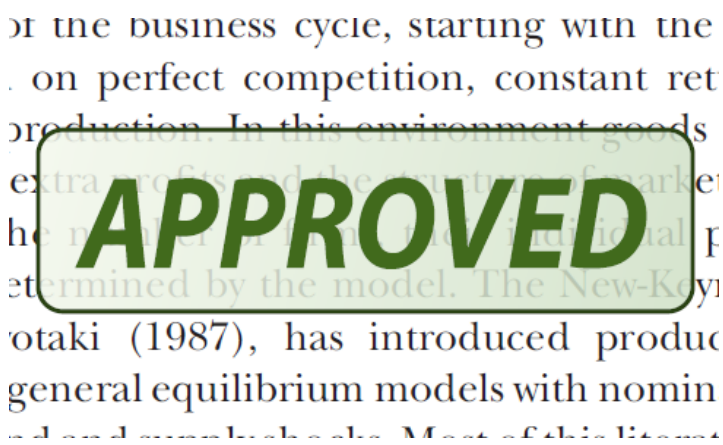

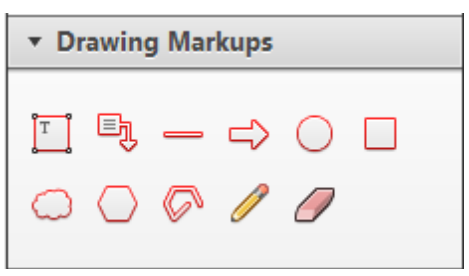

7. Drawing Markups Tools – for drawing shapes, lines and freeform annotations on proofs and commenting on these marks.

Allows shapes, lines and freeform annotations to be drawn on proofs and for comment to be made on these marks..

How to use it

- Click on one of the shapes in the Drawing Markups section.
- Click on the proof at the relevant point and draw the selected shape with the cursor.
- To add a comment to the drawn shape, move the cursor over the shape until an arrowhead appears.
- Double click on the shape and type any text in the red box that appears.

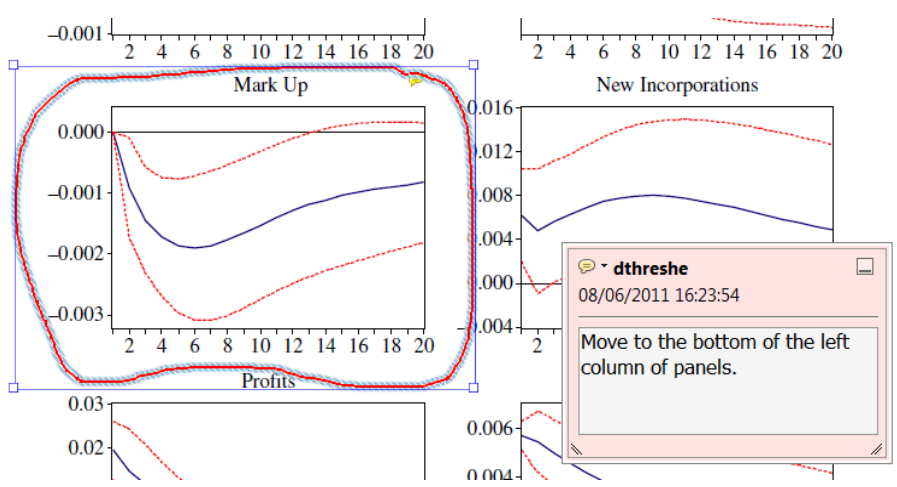

For further information on how to annotate proofs, click on the Help menu to reveal a list of further options:

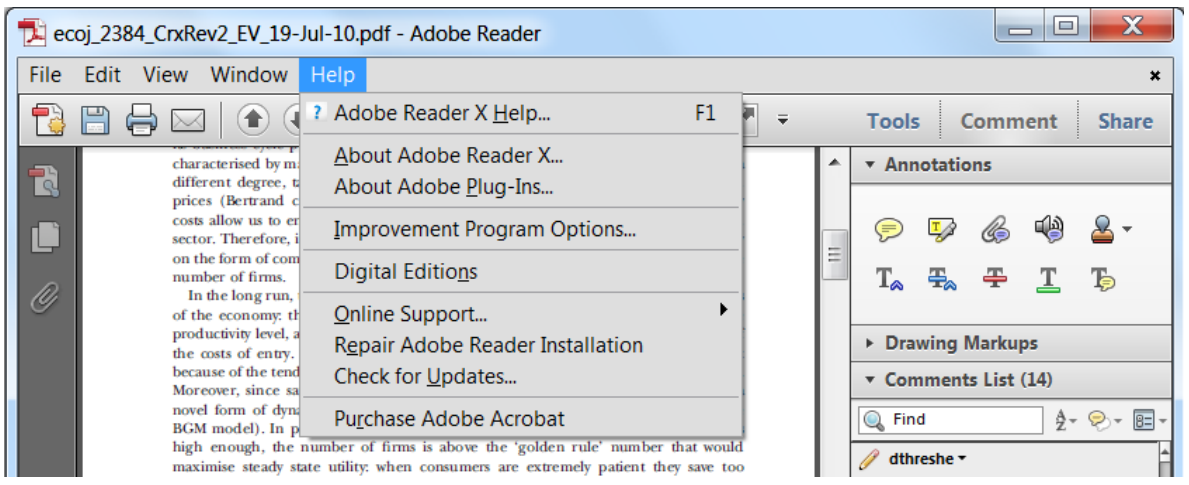

Journal	MSP No.	Dispatch: March 3, 2016	CE: Harshit
JBMR	2815	No. of Pages: 16	PE: Melissa Ekis

ORIGINAL ARTICLE

JBMR®

Heterozygous *PTCH1* Mutations Impact the Bone Metabolism in Patients With Nevoid Basal Cell Carcinoma Syndrome Likely by Regulating SPARC Expression

Yingying Hong,[1] Jianyun Zhang,[1] Heyu Zhang,[2] Xuefen Li,[2] Jiafei Qu,[1] Jiemei Zhai,[1] Lei Zhang,[3] Feng Chen,[2] and Tiejun Li[1]

[1]Department of Oral Pathology, Peking University School and Hospital of Stomatology, Beijing, China
[2]Central Laboratory, Peking University School and Hospital of Stomatology, Beijing, China
[3]Department of Oral Maxillofacial Surgery, Peking University School and Hospital of Stomatology, Beijing, China

ABSTRACT

Nevoid basal cell carcinoma syndrome (NBCCS) is an autosomal dominant disorder characterized by bone and skin abnormalities and a predisposition to various tumors. Keratocystic odontogenic tumors (KCOTs), which are common tumors of the jaw that cause extensive damage to the jawbone, are usually accompanied with NBCCS. Germline *PTCH1* mutations in NBCCS tumorigenesis have been frequently studied; however, little is known regarding the pathogenesis of bone abnormalities in this disease. This study sought to investigate the mechanism underlying heterozygous *PTCH1* mutation-mediated abnormal bone metabolism in patients with NBCCS. Stromal cells were isolated from the fibrous capsules of patients with NBCCS-associated or non-syndromic keratocystic odontogenic tumors and non-syndromic tumor stromal cells without *PTCH1* mutations served as controls. Germline *PTCH1* heterozygous mutations were confirmed in all NBCCS samples and differential protein expression was identified using tandem mass tag-labeled proteomics analysis. Our findings revealed that osteonectin/SPARC expression was significantly downregulated in syndromic stromal cells compared with non-syndromic stromal cells. SPARC expression was even lower in stromal cells carrying *PTCH1* protein truncation mutations. *PTCH1* siRNA transfection demonstrated that SPARC downregulation correlates with decreased PTCH1 expression. Furthermore, exogenous SPARC promoted osteogenic differentiation of syndromic stromal cells with enhanced development of calcium nodules. In addition, bone mineral density tests showed that patients with NBCCS exhibit weak bone mass compared with sex- and age-matched controls. This study indicates that germline *PTCH1* heterozygous mutations play a major role in bone metabolism in patients with NBCCS, in particular in those with *PTCH1* protein truncation mutations. SPARC may represent an important downstream modulator of PTCH1 mediation of bone metabolism. Thus, bone mineral density monitoring is critical for patients with NBCCS for prevention of osteoporosis. In addition, surgical procedures on syndromic-associated KCOTs should be performed with consideration of the weaker bone mass in such patients. © 2016 American Society for Bone and Mineral Research.

KEY WORDS: PTCH1; BONE METABOLISM; NBCCS; SPARC; BONE MINERAL DENSITY

Introduction

Nevoid basal cell carcinoma syndrome (NBCCS; Gorlin syndrome) is an autosomal dominant genetic disorder[1] characterized by multiple dermal and skeletal abnormalities, eg, bifid ribs and falx cerebri calcification, as well as a propensity for various neoplasms such as palmar and plantar pits, multiple nevoid basal cell carcinoma, keratocystic odontogenic tumors, and ovarian fibromas.[2,3] A wide range of skeletal anomalies are observed including in the rib, vertebra, shoulder, and phalanx.[4] Certain major clinical manifestations of NBCCS, such as basal cell carcinomas, keratocystic odontogenic tumors, and falx calcification, are not usually apparent until the teenage years. Therefore, radiological findings of skeletal anomalies (bridging of the sella, bifid rib, polydactyly, widened ends of clavicles) are more significant for the early diagnosis of NBCCS, whereas enhanced surveillance for tumors concomitant with NBCCS, especially skin basal cell carcinoma, medulloblastoma and rhabdomyosarcoma, is necessary in positively diagnosed children as they mature.[5]

Family-based linkage analysis of basal cell carcinomas has identified NBCCS as a dominant hereditary disease.[1] The

Received in original form October 24, 2015; revised form January 23, 2016; accepted February 13, 2016. Accepted manuscript online Month 00, 2016.
Address correspondence to: Tiejun Li, Department of Oral Pathology, Peking University School and Hospital of Stomatology, 22 Zhongguancun Avenue South, Haidian District, Beijing 100081, China. E-mail: litiejun22@vip.sina.com. Feng Chen, Central Laboratory, Peking University School and Hospital of Stomatology, 22 Zhongguancun Avenue South, Haidian District, Beijing 100081, China. E-mail: moleculecf@gmail.com
Additional Supporting Information may be found in the online version of this article.

Journal of Bone and Mineral Research, Vol. 31, No. xx, Month 2016, pp 1–16
DOI: 10.1002/jbmr.2815

human homologue of the *Drosophila* segment polarity gene, *PTCH1*, has been shown to be associated with NBCCS and other tumors.[6,7] *PTCH1*, which has been mapped to chromosome 9q22–31, encodes a highly conserved 12-pass transmembrane protein receptor that functions as a tumor suppressor via negative regulation of the canonical Hh signaling pathway. This pathway is known to function as an important regulator of cell proliferation, fate, and patterning in neural tube and embryonic development[8] by repressing the activity of the G-protein–coupled receptor Smoothened (SMO). Abnormal Hh signaling resulting from loss-of-function mutations in *PTCH1* leads to NBCCS and related tumors, as well as to tumors associated with gain-of-function mutations in SMO.[9,10]

PTCH1 is composed of N- and C-terminal domains, two large extracellular and one large intracellular loops, and 12-pass transmembrane domains, two to six of which form the putative sterol-sensing domain (SSD) considered to participate in vesicular trafficking of cholesterol and other lipids.[11,12] We and other groups have reported that more than 85% of patients with NBCCS harbor heterozygous germline *PTCH1* mutations,[13–15] primarily consisting of PTCH1 protein truncations (73%) that are usually concentrated in the large extracellular and intracellular loops and in the N-terminal region. Germline missense mutations (17%) occur primarily in the transmembrane domains and especially in the SSDs.[16] Loss of heterozygosity of the *PTCH1* gene (>17%) is a common event in patients that are *PTCH1* point mutation-negative. In addition, patients harboring *PTCH1* deletions of less than 2.4 Mb in size do not exhibit phenotypes atypical for NBCCS.[17,18]

To clarify the mechanism underlying the association between heterozygous *PTCH1* mutations/deletions and their associated NBCCS-related phenotypic manifestations, two independent lines of *Ptch1*-deficient mice have been constructed: *Ptch1*$^{+/-}$ (exon 1/2) and *Ptch1*$^{neo\ 67/+}$ mice.[19,20] Both models were found to be prone to tumor development, skeletal abnormalities, and increased susceptibility to irradiation.[21–23] Because Hh-PTCH1 signaling plays a major role in osteoblast differentiation during endochondral bone formation and adult bone homeostasis, in addition to its role in increasing the predisposition to neoplasms, Ohba and colleagues examined bone metabolism in *Ptch1*$^{+/-}$ mice and found that these mice exhibit increased bone mass compared with their wild-type littermates. Moreover, *Ptch1*$^{+/-}$ mice additionally showed enhanced osteoclastogenesis and osteoblast differentiation.[24] In sharp contrast, *PTCH1* gene knockout in mature osteoblasts increased osteoclastogenesis, leading to decreased bone mass and even osteopenia.[25] This contradiction may arise from several factors including impairment in various cell types and developmental stages. In addition, although in vitro studies have shown that activation of Hh signaling inhibits osteoblast differentiation in human mesenchymal stem cells, Hh-PTCH1 signaling is known to differentially affect osteoblast differentiation in human versus rodent mesenchymal cells.[26] Furthermore, conditional knockdown models are not fully representative of inherited *PTCH1* haploinsufficiency in patients with NBCCS who generally exhibit PTCH1 protein truncation and harbor missense mutations. In contrast, *Ptch1* knockout involves complete inactivation of the *Ptch1* gene in knockout mice but does not reflect the pathological state of patients with NBCCS.

To counter these limitations, we isolated heterozygous *PTCH1* mutation-syndromic stromal cells from the fibrous cyst walls of keratocystic odontogenic tumors (KCOTs) associated with NBCCS, and used stromal cells from sporadic KCOTs as controls. As stem cell–like cells, stromal cells from KCOTs exhibit colony-forming and multipotential differentiation ability as well as high self-renewal, and have previously been shown to exhibit decreased osteogenic differentiation and enhanced osteoclastogenesis compared with wild-type stromal cells.[27] In the present study, we performed and compared whole-protein profiles of these stromal cells by tandem mass tag (TMT)-labeled mass spectrometry in order to elucidate the mechanisms by which PTCH1 haploinsufficiency contributes to skeletal anomalies and bone metabolism in patients with NBCCS and to examine the role of PTCH1 in osteoblast differentiation.

Materials and Methods

Patients

For this study, we enrolled 24 patients who were histologically diagnosed with KCOTs from 2012 to 2014 at the Department of Oral and Maxillofacial Surgery at the Peking University School and Hospital of Stomatology (12 with syndromic and 12 with non-syndromic KCOT). Blood specimens and fresh tissues were collected from the patients and a diagnosis of NBCCS was confirmed using published evaluation criteria. NBCCS-associated patients were confirmed using published evaluation criteria[28] defined by the presence of bifid ribs, multiple KCOTs, and basal cell nevus. Clinical characteristics including age, sex, recurrent history, X-ray appearance, and clinical manifestations were obtained from detailed disease history records and careful clinical observations of the patients. Typical clinical characteristics are shown in Fig. 1. All patients provided informed consent, and this study was approved by the Peking University Health and Science Center Ethics Committee.

DNA isolation and PCR

Genomic DNA from stromal cells and peripheral blood samples was extracted using the standard procedure for a QIAGEN DNA Mini Kit (Qiagen, Hilden, Germany). *PTCH1* and *SMO* gene alterations were analyzed by PCR with intronic primers covering 22 coding exons (exons 2 to 23) of *PTCH1* and all *SMO* exons. The PCR reaction mixture (50 μL final volume) contained 25 μL of G2 Green Master Mix (Promega, Madison, WI, USA), 10 nM of each primer, and 100 ng of template DNA. Primer sequences and detailed PCR conditions were as previously described.[29] All amplified products were sequenced using an ABI Prism 3100 Genetic Analyzer (Applied Biosystems, Foster City, CA, USA). Detected mutations were confirmed by both forward and reverse sequencing with at least two independent PCRs.

Cell culture

From 2012 to 2014, we cultured 12 samples of primary syndromic stromal cells derived from primary KCOTs of patients with NBCCS (S-SC) and 12 samples of primary stromal cell-derived cells from non-syndromic KCOTs (NS-SC) that were age- and sex-matched with the NBCCS group. Primary cell culture was performed as previously described.[27] Syndromic and non-syndromic stromal cells were maintained in Alpha MEM (Gibco, Life Technologies, Gaithersburg, MD, USA), supplemented with 15% fetal bovine serum (FBS) (Hyclone, Thermo Fisher Scientific, Waltham, MA, USA), 100 U/mL penicillin/streptomycin (Biosource, Beijing, China), 0.1 mM L-ascorbic acid phosphate (Wako, Osaka, Japan), and 2 mM glutamine (Biosource). Stromal cells grown for five generations or fewer

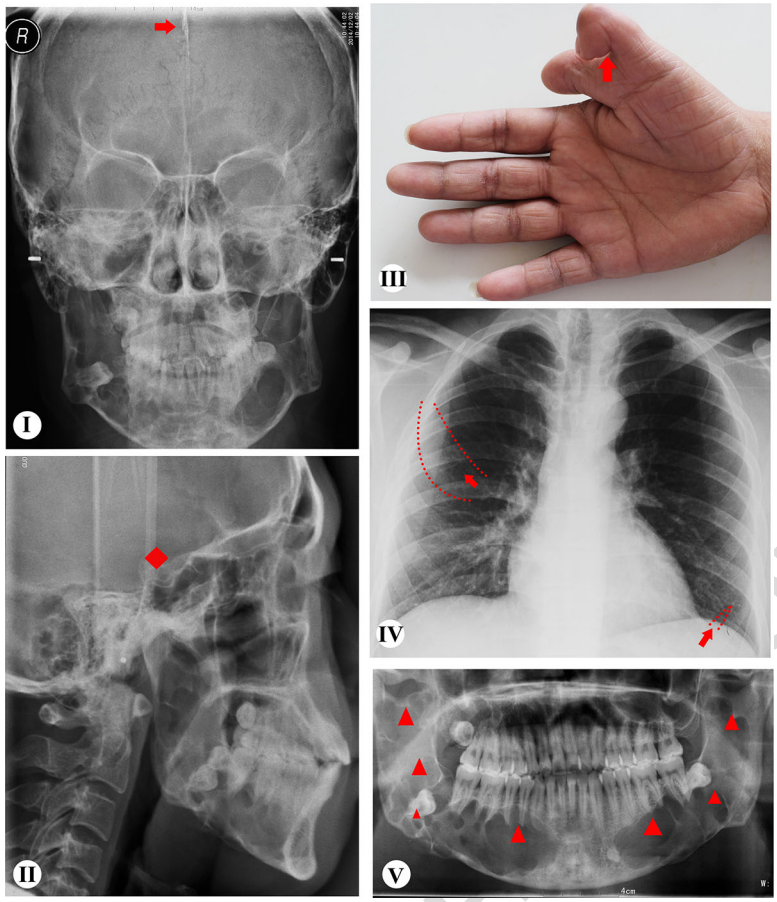

Fig. 1. *PTCH1* mutations and clinical manifestations in 12 patients with NBCCS. Clinical manifestations in patients with NBCCS. (I) Falx cerebri calcification; (II) bone abnormality of the sella turcica region; (III) polydactylism near the base of the right thumb; (IV) abnormality of the ribs: intumescent (arrows) and bifid (dotted line) ribs; (V) multiple KCOTs of the mandible.

were used for subsequent experiments. Human osteoblast-like MG63 cells were purchased from the American Type Culture Collection (ATCC, Manassas, VA, USA) and maintained in Dulbecco's modified Eagle's medium (DMEM) (Gibco[Q5]) containing 10% FBS. All cells were cultured at 37°C in a humidified atmosphere containing 5% CO_2 and 95% air.

siRNA and transfection analysis

MG63 cells were cultured in DMEM supplemented with 10% FBS at 70% confluence in a 6-well plate. For siRNA transfection, 9 μL of RNAiMAX reagent (Life Technologies, Carlsbad, CA, USA) and 30 pmol of siRNA were separately diluted in 150 μL of Opti-MEM medium (Life Technologies). Then, both compounds were mixed, incubated for 5 minutes at 25°C, and the resulting complex was added to the cells. Human *PTCH1* siRNAs and a scrambled non-targeting control siRNA were purchased from Life Technologies (Invitrogen Silencer Select s11441 and s11442, respectively). Knockdown efficiency was determined by real-time quantitative reverse transcription (qRT)-PCR and Western blot analysis 72 hours after transfection (below).

RNA extraction and qRT-PCR

Total RNA was isolated and purified using TRIzol reagent (Life Technologies) and RT-PCR was performed using the RT Master Mix (TaKaRa, Osaka, Japan) based on the manufacturer's instructions. qRT-PCR was performed using the SYBR Green method (Applied Biosystems) in an ABI 7500 thermal cycler. Targeted gene expression was measured using the $2^{-\Delta\Delta Ct}$ method by normalizing to *GAPDH* expression levels. Primer sequences were as previously described.[27]

Protein preparation

The 24 syndromic and matched non-syndromic stromal cell lines were each washed with phosphate-buffered saline, harvested, and lysed in cell lysis buffer containing a protease inhibitor cocktail (Roche, Roswell, GA, USA) and phosphatase inhibitor (Roche) on ice for 30 minutes, then centrifuged at 14,000*g* for 20 minutes at 4°C. The supernatants were collected and the protein concentrations measured using a Pierce BCA Protein Assay Kit (Thermo Scientific).

Proteomics analysis

Equal amount of proteins from each of the 12 samples for each group were mixed together, and the proteins (about 80 mg respectively) were separated by 12% one-dimensional (1D) SDS-PAGE and stained with Coomassie brilliant blue. The gel bands were excised as 12 equal slices corresponding to each group and digested using sequence grade-modified trypsin

(Promega) in 50 mM Na2HPO4 at 37°C overnight. The digested peptides were extracted twice with 1% trifluoroacetic acid in 50% acetonitrile aqueous solution for 30 minutes and then centrifuged in a speedvac to reduce the volume. To quantify the relative differential protein expression between the two groups of cells, tryptic peptides were labeled with TMT reagents (Pierce,[Q6]) according to the manufacturer's instructions. The reaction was incubated for 1 hour at room temperature. Then, 0.5 μL of 5% hydroxylamine (pH 9–10) was added to quench the reaction and incubated for 15 minutes. TMT 127 and 128 were labeled for the non-syndromic and syndromic stromal cells, respectively. Labeled peptides were desalted using Stage tips. For liquid chromatography/mass spectrometry (LC-MS)/MS analysis, the TMT-labeled peptides were separated by a 65-minute gradient elution at a flow rate of 0.250 μL/min using an EASY-nLCII TM integrated nano-HPLC system (Proxeon, Odense, Denmark) interfaced with a Thermo QE mass spectrometer. The analytical column used was a homemade fused silica capillary column (75 μm ID, 150 mm length; Upchurch,[Q7]) packed with C-18 resin (300 A, 5 μm; Varian,[Q8]). The mobile phase A consisted of 0.1% formic acid and mobile phase B consisted of 100% acetonitrile and 0.1% formic acid. The QE mass spectrometer was operated in the data-dependent acquisition mode using X calibur 2.1.2 software with a single full-scan mass spectrum in the orbitrap (400 to 1800 m/z, 60,000 resolution) followed by 10 data-dependent MS/MS scans at 27% normalized collision energy. All MS/MS spectra were searched against the human.fasta UniProt database using an in-house Proteome Discoverer (Version PD1.4, Thermo-Fisher Scientific). Peptides with charge scores >4.5 were used for protein identification. The detailed search criteria used were as described previously.[30] Ratios of 128:127 for each protein were calculated using the median of all peptide hits corresponding to a given protein. The ratios of two or more tryptic peptides from the same protein were used to calculate the means and standard deviations.

Western blot analysis

Differential protein expression between the two cell groups was confirmed by Western blotting and further verified using independent samples. SiRNA-transfected cells were harvested at 72 hours after transfection. Whole-cell proteins were extracted as described above and subjected to 12% SDS-PAGE followed by transfer onto a PVDF membrane (Millipore, Billerica, MA, USA). Membranes were blocked with 5% skim milk for 1 hour at room temperature and incubated with primary antibodies (β-actin: 1:1000 [Santa Cruz Biotechnology, Dallas, TX, USA], SPARC: 1:1000 [Cell Signaling Technology, Danvers, MA, USA], PTCH1: 1:1000 [Abcam, Cambridge, UK]) overnight with shaking at 4°C. Membranes were then washed three times with Tris buffered saline-Tween 20 for 5 minutes. Then, secondary anti-mouse or anti-rabbit (Cell Signaling Technology) antibodies were added and incubated at room temperature for 1 hour. After washing, immunoreactive proteins were detected using an enhanced chemiluminescence (ECL) reagent (Applygen Technology, Beijing, China).

Immunohistochemistry

From 2010 to 2014, an additional 100 pathological specimens from patients pathologically diagnosed with KCOTs at the Department of Pathology, Peking University School of Stomatology, were utilized in this study to validate differential protein expression in tissues. These cases comprised 42 syndromic KCOTs and 58 non-syndromic KCOTs without clinical syndromic manifestations. We prepared 4-μm paraffin-embedded tissue sections on charged glass slides for staining. Slides were dewaxed using a gradient ethanol series and then blocked for endogenous peroxidase activity in 3% hydrogen peroxide/methanol buffer for 20 minutes. Antigen retrieval was performed using a high-pressure method with sodium citrate buffer (pH 6.0). After washing, goat serum was used as a blocking agent for 20 minutes, and then slides were incubated with a rabbit anti-human osteonectin antibody, used as supplied, (Zhongshan Golden Bridge, Zhongshan, China) in a humidified chamber overnight at 4°C. Primary antibody was detected using a horseradish peroxidase-conjugated secondary antibody (Zhongshan Golden Bridge) for 30 minutes at 25°C. After rinsing, the immunoreaction was visualized by incubation with 3,3′-diaminobenzidine (Zhongshan Golden Bridge) for 1 minute. Slides were counterstained with hematoxylin and observed using an Olympus DP controller (Olympus, Tokyo, Japan). The staining results were evaluated by two independent investigators who were blinded to specimen information. The labeling index was defined as the intensity of staining (strong, moderate, weak, and negative, scored as 4, 3, 2, and 1, respectively) and multiplied by the percentage of positive cells (0, 25%, 50%, or 75%).

Osteogenic differentiation

Syndromic and non-syndromic stromal cells from the same passages were seeded in 24-well and 6-well plates. Osteogenesis induction medium supplemented with 15% FBS, 10 nM dexamethasone, 50 μg/mL l-ascorbic acid-2-phosphate, and 10 mM β-glycerophosphate (Sigma-Aldrich, St. Louis, MO, USA) was replaced when cells were at 70% confluence. The experimental group was treated with 0.5 μg/mL of recombinant human SPARC/osteonectin (Sigma) diluted in 0.1% BSA buffer, and the parallel control group was treated with buffer alone. The induction medium containing human ectogenous SPARC/osteonectin was exchanged 3 times per week. Total protein was extracted after 1-week induction for determination of alkaline phosphatase (AKP) activity using an AKP activity kit (Nanjing Jiancheng Bioengineering Institute, China) in accordance with the manufacturer's instructions. The expression of osteoblast-specific genes was measured by qRT-PCR 2 weeks later. Three weeks after induction, cells were fixed and stained with 1% alizarin red S (Sigma) for observation of calcium nodus formation.

Bone mineral density (BMD) analysis

From 2013 to 2015, 12 patients with NBCCS who had provided informed consent participated in BMD analysis. BMD was determined by dual-energy X-ray absorptiometry (DXA; HOLOGIC Discovery A, Bedford, MA, USA) in the Bone Density Examination Room of the Peking University Third Hospital. The BMD (g/cm^2) at the posteroanterior lumbar spine (L_1 to L_4) and femoral neck (FN) were measured. *Z*-scores and *T*-scores were both calculated using the manufacturer's reference data by contrasting individual BMD parameters of the patients against those of age- and sex-matched controls. Osteopenia and osteoporosis were confirmed by *T*-scores of < -1 and < -2.5 according to World Health Organization (WHO) criteria.[31]

Statistical analysis

All assays were performed in triplicate and repeated at least three times. We performed the ShapiroWilk test to test the normality of all values. The Student's *t* test and one-way ANOVA (Tukey and S-N-K) were applied to calculate the statistical significance of the results using SPSS 19.0 (SPSS, Chicago, IL, USA). Western blot analyses were performed on multiple samples several times, normalized to β-actin levels using grayscale scanning, and quantified using Image J software (National Institutes of Health). Results were further summarized and graphed using Prism version 5.04 software (Graph Pad, La Jolla, CA, USA). A p value < 0.05 was considered statistically significant ($^{*}p < 0.05$; $^{**}p < 0.01$; $^{***}p < 0.001$). The results of each experiment were presented as means ± SD.

Results

PTCH1 mutational analysis in syndromic and non-syndromic KCOTs

PTCH1 and *SMO* gene mutations were studied in 12 syndromic and 12 non-syndromic stromal cells and associated peripheral blood samples by direct sequencing. We detected 13 *PTCH1* mutations in 12 syndromic stromal cell lines, all of which were consistent with the mutations detected in the DNA from the respective blood samples (Table 1). Of these, three represented novel mutations. One in-frame indel (c.3403_3405del3) resulted in the deletion of a leucine residue between codons 3402 and 3406. Two frameshifts (c.2172delC, c.1348_1351delCTCG) introduced stop codons at amino acid residues 724 and 451, respectively. The two mutations carried by patient NB2 (as shown in Table 1) were confirmed as being located on the same allele. Overall, 66.7% of the mutations resulted in a stop codon, which generated PTCH1 protein truncations at various locations. The concordance between the findings in the stromal cells and the blood samples indicated that the heterozygous mutations likely occurred at the germline level. Additionally, we identified 18 previously described *PTCH1* gene polymorphic sites in non-syndromic stromal cells, as well as 23 previously described *SMO* polymorphisms in both groups (data not shown).

Differential protein expression between syndromic and non-syndromic stromal cells

Equivalent protein amounts from mixtures of syndromic or non-syndromic stromal cells were separated by SDS-PAGE and the protein profiles were examined using proteomics analysis. The TMT labeling method was applied to filter differentially expressed proteins. More than 1800 proteins were identified in both cell mixtures. Under the selection criteria of false-discovery rate $<1\%$, TMT ratio >2.0 or <0.6, and protein confidence $>95\%$, a total of 111 proteins (98 downregulated and 13 upregulated proteins) exhibited significantly different expression between syndromic and non-syndromic stromal cells based on UniProt human.fasta database search (Fig. 2*A*). Gene ontology (GO) was classified according to biological process, based on differentially expressed proteins between the two groups (Fig. 2*B*). GO results are shown according to the significance level of the different biological processes, including mRNA metabolism, cellular protein metabolism, regulation of apoptosis, vesicle-mediated transport, and ossification, the latter category containing multiple types of ossification. Notably, three biological processes related to ossification (endochondral ossification, intramembranous ossification, and ossification itself) were identified. Details of differentially expressed proteins are listed in Table 2.

SPARC protein expression is significantly lower in syndromic than in non-syndromic stromal cells

In accordance with the results of GO analysis, we focused our research on ossification-related proteins, especially secreted protein acidic and cysteine-rich osteonectin/SPARC. According to the TMT-labeling ratio, SPARC was 0.6-fold downregulated in syndromic stromal cells compared with non-syndromic stromal cells. The downregulated expression in syndromic stromal cells was verified by Western blot. First, mixtures of S-SC cells were confirmed to exhibit 55.2% lower SPARC expression than cells in the NS-SC group ($p = 0.002$, $n = 3$) (Fig. 3*A*). To validate SPARC expression in individual patients, we tested protein expression in independent samples from sex- and age-matched syndromic and non-syndromic stromal cells. The results showed the same trend, with significantly lower SPARC expression in stromal cells derived from patients with NBCCS who carried mutations resulting in PTCH1 truncation. In addition, the results revealed that SPARC expression in stromal cells from patients with non-truncating mutations was weaker than, or did not significantly differ from, expression in corresponding controls (Fig. 3, $p = 0.004$, $n = 12$) (Fig. 3*B*). To study SPARC expression patterns in KCOT tissues, we immunohistochemically stained 100 KCOT specimens including those from 42 patients with NBCCS-associated KCOTs and 58 with sporadic KCOTs. SPARC expression was observed in the cytoplasm of fibrous cystic-wall cells and vascular endothelial cells; in particular, areas within the peripheral region of the cystic wall where in close contact with the bone destructive and absorptive surface showed enhanced SPARC staining. Staining was obviously stronger and more extensive in non-syndromic KCOT samples than in syndromic KCOTs (Fig. 3*C*). The results were consistent with those from Western blotting.

PTCH1 knockdown downregulates SPARC expression

To clarify the reason underlying SPARC downregulation in S-SCs, we silenced *PTCH1* in MG63 cells using siRNA transfection. Two siRNA constructs were used to knock down PTCH1, and silencing efficiency was tested by qRT-PCR and Western blot. The results showed that both siRNA constructs reduced *PTCH1* mRNA levels by 78% and 84%, respectively, compared with that in cells transfected with negative control ($p = 0.003$, $p = 0.004$, $n = 3$) (Fig. 4*A*). Similarly, PTCH1 protein expression was downregulated by more than 50.4% compared with the control, in addition to a significant concomitant reduction (by more than 53.9%) in SPARC protein levels, indicating that SPARC and PTCH1 expression are correlated (Fig. 4*B*).

Exogenous SPARC promoted osteogenic differentiation in syndromic and non-syndromic stromal cells separately

To identify whether SPARC promotes osteoinductive differentiation, we expressed SPARC exogenously in syndromic and non-syndromic stromal cells to stimulate osteogenetic differentiation. We examined changes in AKP activity, mRNA levels, and mineralized nodule formation at the first, second, and third week, respectively, during induction. AKP activity tests showed that the AKP activity of S-SC cells stimulated by exogenous SPARC was nonsignificantly elevated by 1.13-fold

Table 1. PTCH1 Mutations in 12 Patients With NBCCS

Patient	Age/sex	Exon	Nucleotide change	Amino acid definition	Mutation type	Germline	Phenotype	N-terminus
NB 1	16/F	Exon3	c.403C>T[a]	*p.Arg135**	Nonsense	Same	Multiple KCOTs, bifid rib, palmar pits, recurrent history	ECL1
NB 2	32/F	Exon3	c.403C>T[a]	*p.Arg135**	Nonsense	Same	Multiple KCOTs, calcification of falx cerebri, bridged sella, frontal bossing,	ECL1
		Exon17	c.2824delC[a]	*p.Arg942Glyfs*20*	Frameshift	Same	palmar/planter pits, multiple skin nevi, recurrent history	ECL4
NB 3	60/F	Exon3	c.403C>T[a]	*p.Arg135**	Nonsense	Same	Multiple KCOTs, multiple skin nevi, bifid rib, calcification of falx cerebri, palmar pits, fundus oculi disease, telecanthus, recurrent history	ECL1
NB 4	15/M	Exon2	c.233G>A[a]	*p.Trp78**	Nonsense	Same	Multiple KCOTs, multiple skin nevi, cleft lip and palate, calcification of falx cerebri, palmar pits, recurrent history	N-terminus
NB 5	30/M	Exon20	c.3403_3405delCTC[b]	*p.Leu1135del*	Inframe indel	Same	Multiple KCOTs, bifid rib, protopsis, icteric sclera, thoracocyllosis, recurrent history	TM11
NB 6	45/M	Exon2	c.233G>A[a]	*p.Trp78**	Nonsense	Same	Multiple KCOTs, multiple skin nevi, cleft lip and palate, calcification of falx cerebri, palmar pits, recurrent history	N-terminus
NB 7	20/F	Exon14	c.2179delT[a]	*p.Cys727Valfs*13*	Frameshift	Same	Multiple KCOTs, palmar/planter pits, frontal bossing, telecanthus, reccurent history	TM7
NB 8	16/M	Exon14	c.2172delC[b]	*p.Gln724Glyfs*21*	Frameshift	Same	Multiple KCOTs, calcification of falx cerebri, palmar pits, skin yellowing sclera, thoracocyllosis, recurrent history	ICL3
NB 9	17/M	Exon11	c.1526G>A[a]	*p.Gly509Asp*	Missense	Same	Multiple KCOTs, multiple skin nevi, recurrent history	TM4
NB 10	27/M	Exon10	c.1348_1351delCTCG[b]	*p.Ala451Profs*39*	Frameshift	Same	Multiple KCOTs, multiple skin nevi, bifid rib, palmar pits, frontal bossing	TM3
NB 11	18/M	Exon21	c.3499G>A[a]	*p.Gly1167Arg*	Missense	Same	Multiple KCOTs, multiple skin nevi, calcification of falx cerebri, palmar pits, bifid rib	TM12
NB 12	17/M	Exon21	c.3499G>A[a]	*p.Gly1167Arg*	Missense	Same	Multiple KCOTs, multiple skin nevi, palmar pits, bifid rib, frontal bossing, conjunctival congestion, icteric sclera, thoracocyllosis, recurrent history	TM12

NB = NBCCS case.
[a]PTCH1 mutations were previously reported by our group 6–8.
[b]PTCH1 mutations were detected in the present study.

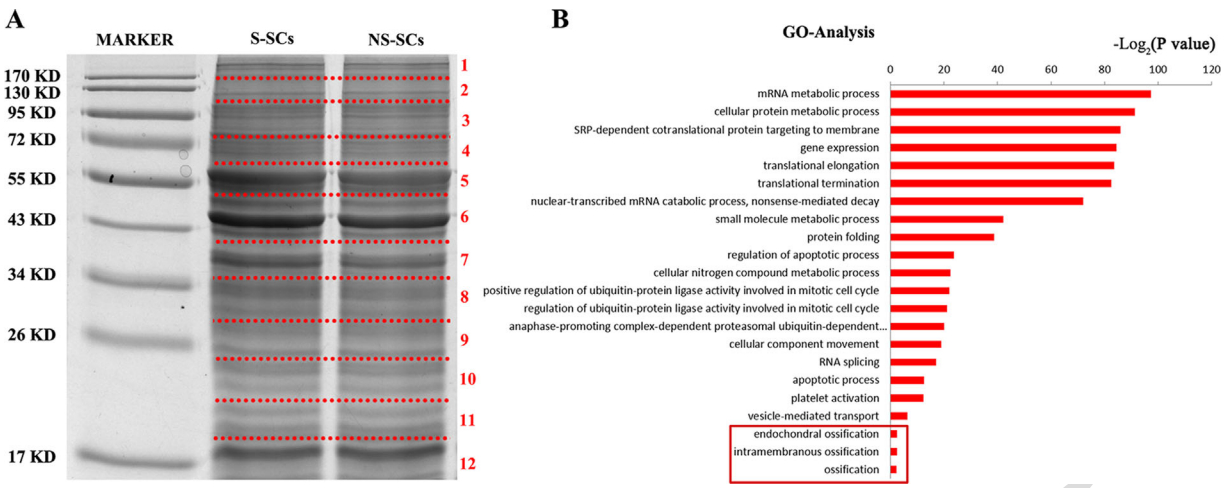

Fig. 2. Differentially expressed proteins in S-SCs and NS-SCs. (*A*) SDS-PAGE analysis of S-SC and NS-SC cells. (Lane 1) protein markers; (lane 2) protein from S-SC cells; (lane 3) protein from NS-SC cells; each protein lane was divided into 12 bands as shown. (*B*) Proteins exhibiting significant differential expression between S-SCs and NS-SCs were classified by GO analysis, which is shown according to the significance level of the various biological processes.

over that of the corresponding control ($p = 0.796$, $n = 6$), whereas that of stimulated NS-SC cells was enhanced 1.62 times ($p = 0.042$, $n = 6$) at the first week of induction (Fig. 5*A*). Furthermore, mRNA expression analysis of osteogenesis-related genes revealed that *OPN* expression was 4.5-fold higher in SPARC-stimulated cells than in nonstimulated S-SC cells ($p = 0.016$, $n = 6$) and that *COL1A1*, *OCN*, and *RUNX2* showed no significant differences in expression between the two groups. In NS-SC cells, the mRNA levels corresponding to *OCN*, *OPN*, and *RUNX2* were respectively 2.21-, 4.2-, and 2.33-fold upregulated in the stimulated group ($p = 0.02$, 0.007, 0.03, respectively; $n = 6$) (Fig. 5*B*). Correspondingly, alizarin red staining was found to be more intense and calcium nodes were enhanced when both type cells were induced by exogenous SPARC added to the induction medium. Accordingly, calcium node formation in NS-SC cells showed stronger osteogenic effects in response to exogenous SPARC than in S-SC cells (Fig. 5*C*). Therefore, we concluded that exogenous SPARC promotes osteoblast differentiation in both syndromic stromal cells and non-syndromic stromal cells, to different degrees, separately in vitro, and that non-syndromic stromal cells exhibit greater sensitivity to SPARC stimulation.

Low BMD was correlated with *PTCH1* mutations in patients with NBCCS

To clarify whether *PTCH1* mutations affect the BMD of patients with NBCCS, we recruited 12 male patients with NBCCS for BMD scanning from 2013 to 2015 to exclude the influence of estrogenic hormones on bone mass. The recruited patients were aged 16 to 60 years, with an average age of 32.9 years. BMD scanning was performed at the Peking University Third Hospital by the same radiologist. According to WHO criteria for osteopenia, a *T*-score between −2.5 and −1.0 is linked to elevated risk of fracture and a diagnosis of osteopenia. Our results showed that 4 of the 12 patients in different age groups suffered from osteopenia, yielding an incidence rate of approximately 33.3%. Furthermore, the *T*-scores of another 4 patients were close to −1.0 and their bone masses were low compared with an age- and sex-matched reference population. The *T*-scores of the other 4 patients fluctuated above and below zero and their bone masses were at the mid-range of the control population (shown in Fig. 6). Our results indicate that patients with NBCCS are prone to low BMDs and may therefore suffer an enhanced risk of fracture at various age ranges.

Discussion

NBCCS is an autosomal dominant disorder associated with an increased disposition toward defects of the skeleton, skin, and nerves. In addition, the development of various tumors (predominantly multiple nevoid basal cell carcinomas and KCOTs) in the second decade of life are common.[2,3] Defects, such as falx cerebri calcification, sella turcica region dysplasia, bifid ribs, and polydactyly, which may be widely distributed over the skeleton (the skull, vertebrae, ribs, and limb bones), are crucial for early childhood diagnosis of NBCCS in families with an increased incidence of the disease. Such early diagnosis is essential for tumor surveillance throughout the lifetime of the patient.

KCOTs (previously, odontogenic keratocysts) are the most common benign jaw neoplasm, as redefined by WHO in 2005, with a high growth potential and propensity for recurrence.[32] KCOTs usually occur as solitary lesion or as multiple lesions associated with NBCCS. The KCOTs exhibit different clinical manifestations; syndromic-associated KCOTs are usually numerous and associated with larger levels of bone destruction and higher recurrence rates, whereas solitary KCOTs generally occur as single tumors and are associated with limited bone destruction. Among the diverse clinical features observed in patients with NBCCS, KCOTs are frequently the first manifestation to be detected and are diagnosed by oral and maxillofacial surgeons. Our group has previously isolated stromal cells from surgically excised KCOTs, which have been demonstrated to exhibit bone marrow mesenchymal stem cell–like characteristics.[27] Through direct DNA sequencing analysis, we determined that stromal cells and blood samples from an

Table 2. Differentially Expressed Proteins in S-SCs and NS-SCs

Accession	Description	Score	Coverage (%)	Unique peptides	Ratio (S-SC/NS-SC)
IPI00455315.4	Isoform 1 of annexin A2	160.68	68.14	24	0.43
IPI00032140.4	Serpin H1	104.06	39.71	11	0.36
IPI00465248.5	Isoform alpha-enolase of Alpha-enolase	96.02	44.93	15	0.46
IPI00010796.1	Protein disulfide-isomerase	91.81	47.83	21	0.39
IPI00304962.4	Collagen alpha-2(I) chain	90.53	25.99	23	0.51
IPI00303476.1	ATP synthase subunit beta, mitochondrial	84.65	37.81	12	0.37
IPI00329801.12	Annexin A5	66.70	40.63	10	0.41
IPI00419833.9	Histone H2B type 1-K	65.61	57.14	2	0.26
IPI00018534.4	Histone H2B type 1-L	64.83	57.14	2	0.23
IPI00020599.1	Calreticulin	61.54	48.20	16	0.38
IPI00465084.6	Desmin	60.84	11.28	2	0.48
IPI01012004.1	cDNA PSEC0175 fis, clone OVARC1000169, highly similar to protein disulfide-isomerase A3	58.28	31.46	12	0.34
IPI00784154.1	60 kDa heat shock protein, mitochondrial	57.89	22.86	8	0.45
IPI00216138.6	Transgelin	55.82	47.76	10	0.20
IPI00797270.4	Isoform 1 of triosephosphate isomerase	50.27	66.67	12	0.48
IPI01013559.1	cDNA FLJ58502, highly similar to protein disulfide-isomerase A6	49.36	24.71	9	0.37
IPI00218918.5	Annexin A1	43.07	28.03	8	0.42
IPI00219219.3	Galectin-1	41.43	79.26	8	0.48
IPI00419585.9	Peptidyl-prolyl cis-trans isomerase A	40.69	50.91	10	0.34
IPI00014581.1	Isoform 1 of tropomyosin alpha-1 chain	38.36	29.58	1	0.42
IPI00335168.9	Isoform non-muscle of myosin light polypeptide 6	37.70	41.06	5	0.31
IPI00924593.1	cDNA FLJ52880, highly similar to malate dehydrogenase, mitochondrial	37.10	38.18	8	0.51
IPI00930144.1	Histone H2A	36.93	29.73	2	0.16
IPI00010779.4	Isoform 1 of tropomyosin alpha-4 chain	36.90	35.48	5	0.46
IPI00471928.6	ATP synthase subunit alpha	36.39	22.47	9	0.37
IPI00021263.3	14-3-3 protein zeta/delta	35.92	47.76	8	0.52
IPI00216135.1	Isoform 3 of tropomyosin alpha-1 chain	33.46	27.46	1	0.50
IPI00797148.1	Isoform 2 of heterogeneous nuclear ribonucleoprotein A1	32.94	30.71	6	0.47
IPI00939560.1	Thioredoxin domain-containing protein 5 isoform 3	31.55	17.90	5	0.38
IPI00302944.3	Isoform 4 of collagen alpha-1(XII) chain	31.45	5.56	10	0.53
IPI00013895.1	Protein S100-A11	30.85	80.00	6	0.51
IPI00008530.1	60S acidic ribosomal protein P0	29.61	36.59	7	0.49
IPI00025512.2	Heat shock protein beta-1	28.86	25.85	4	0.45
IPI00296099.6	Thrombospondin-1	27.05	6.67	6	0.53
IPI00479185.1	Tropomyosin alpha-3 chain isoform 4	26.72	37.10	4	0.49
IPI00413344.3	Cofilin-2	24.02	33.13	1	0.54
IPI01014936.1	cDNA FLJ35087 fis, clone PLACE6005546, highly similar to polymerase I and transcript release factor	23.58	23.77	8	0.29

Table 2. (*Continued*)

Accession	Description	Score	Coverage (%)	Unique peptides	Ratio (S-SC/NS-SC)
IPI00295400.1	Isoform 1 of tryptophanyl-tRNA synthetase, cytoplasmic	22.12	12.53	4	0.37
IPI01011809.1	RTN4 protein	21.93	8.41	2	0.54
IPI00334174.3	Isoform 2 of Ras-related protein Rab-1A	21.44	31.21	1	0.28
IPI00000816.1	Isoform 1 of 14-3-3 protein epsilon	21.21	26.27	3	0.45
IPI00788837.2	cDNA FLJ54752, highly similar to poly(rC)-binding protein 2	20.58	19.15	4	0.50
IPI00216308.5	Voltage-dependent anion-selective channel protein 1	20.24	26.86	6	0.49
IPI01014727.1	cDNA FLJ51983, highly similar to phosphoglycerate mutase 1	20.21	29.29	7	0.51
IPI00640006.1	rab GDP dissociation inhibitor beta isoform 2	19.36	14.50	5	0.40
IPI00011229.1	Cathepsin D	18.77	11.41	4	0.42
IPI00967527.1	ENC-1AS	18.62	25.38	6	0.46
IPI00026260.1	Isoform 1 of nucleoside diphosphate kinase B	18.17	38.16	4	0.49
IPI01015994.1	cDNA FLJ51779, highly similar to vacuolar ATP synthase subunit B, brain isoform	17.60	19.48	4	0.43
IPI00910779.1	cDNA FLJ52141, highly similar to 14-3-3 protein gamma	17.54	28.02	3	0.53
IPI00744692.1	Transaldolase	17.32	15.43	5	0.51
IPI00956601.1	UDP-glucose 6-dehydrogenase isoform 2	16.78	7.49	3	0.47
IPI00015262.10	Calponin-2	16.76	17.80	4	0.44
IPI00414696.1	Isoform A2 of heterogeneous nuclear ribonucleoproteins A2/B1	17.30	20.53	5	0.48
IPI00006865.4	Vesicle-trafficking protein SEC22b	17.01	23.26	5	0.29
IPI00298547.3	Protein DJ-1	16.90	34.39	5	0.17
IPI00289800.7	Isoform short of glucose-6-phosphate 1-dehydrogenase	16.70	14.37	6	0.45
IPI00009236.5	Isoform alpha of caveolin-1	16.63	29.21	4	0.17
IPI00026530.4	Protein ERGIC-53	16.26	13.14	4	0.32
IPI00554786.5	Isoform 5 of thioredoxin reductase 1, cytoplasmic	16.17	14.63	4	0.35
IPI00220362.5	10 kDa heat shock protein, mitochondrial	16.07	60.78	6	0.53
IPI00016513.5	Ras-related protein Rab-10	15.55	17.00	2	0.25
IPI00759663.1	Isoform cytoplasmic+peroxisomal of peroxiredoxin-5, mitochondrial	15.08	48.15	5	0.44
IPI00956684.1	Galectin-3 isoform 2	14.99	13.00	2	0.29
IPI00909207.1	cDNA FLJ60461, highly similar to peroxiredoxin-2	14.80	19.67	3	0.25
IPI00018146.1	14-3-3 protein theta	14.71	21.63	2	0.49
IPI01014579.1	cDNA FLJ59133, highly similar to cathepsin B	14.71	14.29	2	0.30
IPI00793443.2	Isoform 1 of importin-5	14.47	2.64	2	0.52
IPI00642548.2	Phosphoglycerate dehydrogenase	14.35	10.82	5	0.34
IPI00028055.4	Transmembrane emp24 domain-containing protein 10	14.32	22.37	5	0.22
IPI00219037.5	Histone H2A.x	14.28	26.57	2	0.32
IPI00909534.1	cDNA FLJ59433, highly similar to elongation factor 1-gamma	14.22	11.65	2	0.47
IPI00930720.2	Ras-related protein Rab-11A isoform 2	14.03	27.74	4	0.27
IPI00646304.4	Peptidyl-prolyl cis-trans isomerase B	13.72	28.24	8	0.07

Table 2. (*Continued*)

Accession	Description	Score	Coverage (%)	Unique peptides	Ratio (S-SC/NS-SC)
IPI00220739.3	Membrane-associated progesterone receptor component 1	13.48	22.56	3	0.20
IPI01015100.1	Membrane-associated progesterone receptor component 2	12.93	12.56	1	0.27
IPI00016342.1	Ras-related protein Rab-7a	12.89	23.19	4	0.37
IPI00010896.3	Chloride intracellular channel protein 1	12.79	29.88	5	0.48
IPI00411704.9	Isoform 1 of eukaryotic translation initiation factor 5A-1	12.58	24.03	3	0.47
IPI00024920.1	ATP synthase subunit delta, mitochondrial	12.53	13.69	2	0.44
IPI00219757.13	Glutathione S-transferase P	12.48	27.62	4	0.26
IPI00012048.1	Isoform 1 of nucleoside diphosphate kinase A	12.46	20.39	1	0.18
IPI00017704.3	Coactosin-like protein	12.30	30.28	4	0.50
IPI00980175.1	Proteasome subunit beta type-2 isoform 3	12.25	55.95	3	0.22
IPI00217465.5	Histone H1.2	12.00	21.13	2	0.39
IPI00895865.1	Electron transfer flavoprotein subunit alpha, mitochondrial isoform b	11.93	10.21	2	0.48
IPI00216319.3	14-3-3 protein eta	11.87	15.85	1	0.41
IPI01015962.1	cDNA FLJ50711, moderately similar to ras-related protein Rap-1b	11.80	37.32	5	0.14
IPI00759832.1	Isoform short of 14-3-3 protein beta/alpha	11.61	16.80	1	0.39
IPI00333015.7	Isoform 2 of spectrin beta chain, brain 1	11.50	2.13	4	0.51
IPI00219622.3	Proteasome subunit alpha type 2	11.21	20.09	3	0.41
IPI01011075.1	Superoxide dismutase	11.19	17.28	2	0.15
IPI00024933.3	Isoform 1 of 60S ribosomal protein L12	10.87	26.06	3	0.22
IPI00179964.5	Isoform 1 of polypyrimidine tract-binding protein 1	10.73	6.21	2	0.41
IPI00182373.2	Isoform IIa of Prolyl 4-hydroxylase subunit alpha-2	10.70	10.13	3	0.35
IPI00555577.1	Thy-1 cell surface antigen variant (fragment)	10.61	26.90	3	0.35
IPI00922290.1	cDNA FLJ53094, highly similar to receptor expression-enhancing protein 5	10.56	13.46	3	0.52
IPI00016339.4	Ras-related protein Rab-5C	10.31	16.67	2	0.25
IPI00031522.2	Trifunctional enzyme subunit alpha, mitochondrial	6.74	4.59	2	1.38
IPI00893179.1	X-ray repair complementing defective repair in Chinese hamster cells 6	6.53	5.21	3	1.41
IPI00010418.6	Isoform 2 of myosin-Ic	16.27	4.86	3	1.41
IPI00291175.7	Isoform 1 of vinculin	65.10	18.86	16	1.43
IPI00220466.1	Isoform 3 of LIM domain and actin-binding protein 1	7.21	6.35	2	1.50
IPI00003865.1	Isoform 1 of heat shock cognate 71 kDa protein	63.81	34.52	19	1.56
IPI00009904.1	Protein disulfide-isomerase A4	10.62	6.36	2	1.59
IPI00414676.6	Heat shock protein HSP 90-beta	39.57	15.33	10	1.68
IPI00003362.3	78 kDa glucose-regulated protein	71.01	35.78	19	1.73
IPI00300562.2	Ras-related protein Rab-3B	12.04	8.22	1	1.85
IPI00219301.7	Myristoylated alanine-rich C-kinase substrate	10.01	14.46	3	1.85
IPI00377087.4	Gelsolin	9.92	18.62	2	1.90
IPI00219365.3	Moesin	29.27	12.48	8	1.96

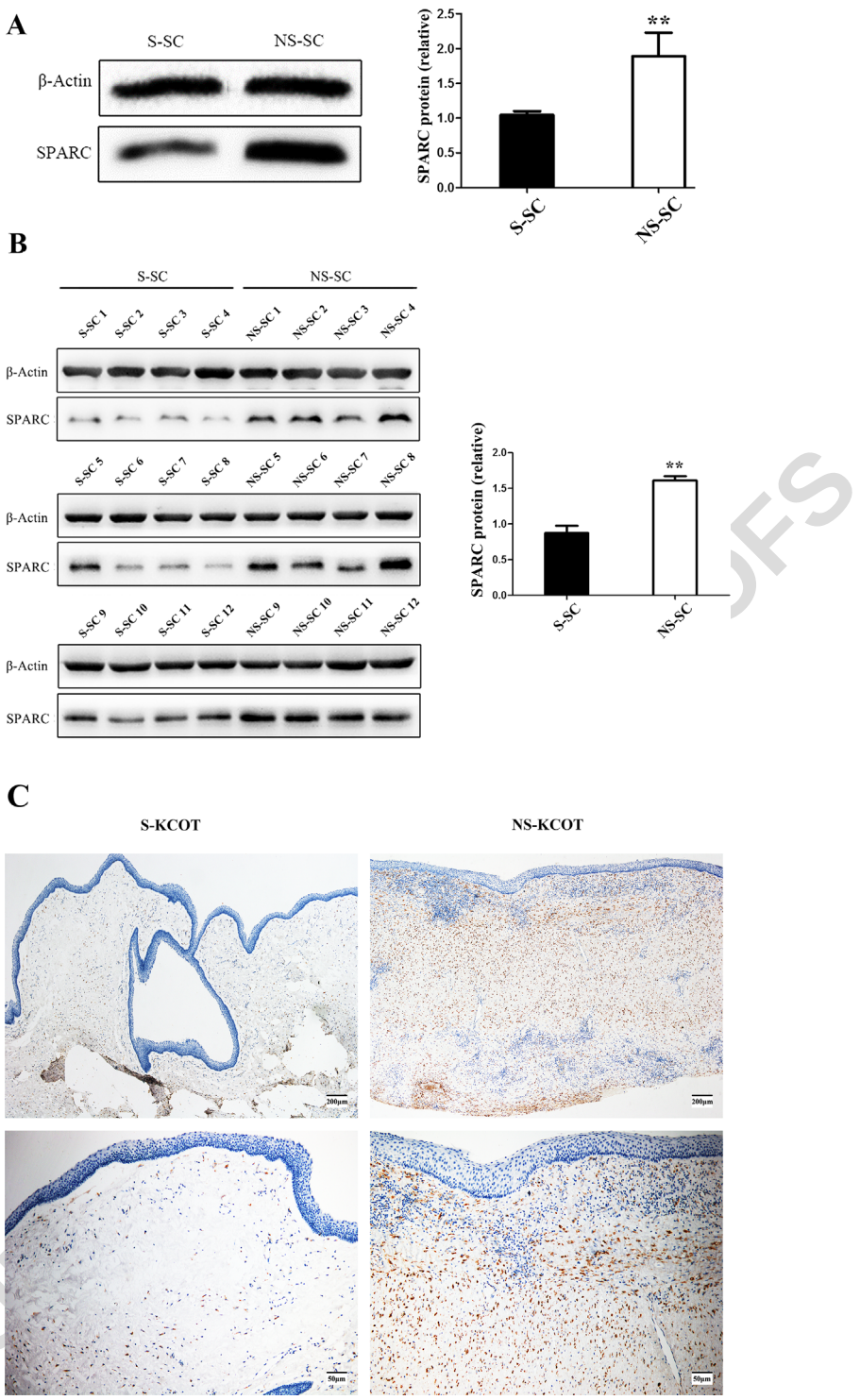

Fig. 3. Verification of lower SPARC expression in S-SCs compared with NS-SCs by Western blot and immunohistochemistry. (*A*) S-SC and NS-SC cell mixtures were separated by SDS-PAGE and analyzed by Western blot using a SPARC antibody and actin as a control. The grayscale values of the bands were scanned using Image J software, and error bars are presented as means ± SEM. $^{**}p < 0.01$ ($n = 3$ technical replicates). (*B*) Independent samples of S-SC and corresponding sex- and age-matched NS-SCs cells were further examined by Western blot ($n = 12$). The detailed *PTCH1* mutation locations are listed in Fig. 1*B*. Error bars are presented as means ± SEM. $^{**}p < 0.01$. (*C*) SPARC staining can be observed in the fiber capsules of KCOTs and in stromal cell cytoplasm. NS-KCOTs showed enhanced staining compared with S-KCOTs.

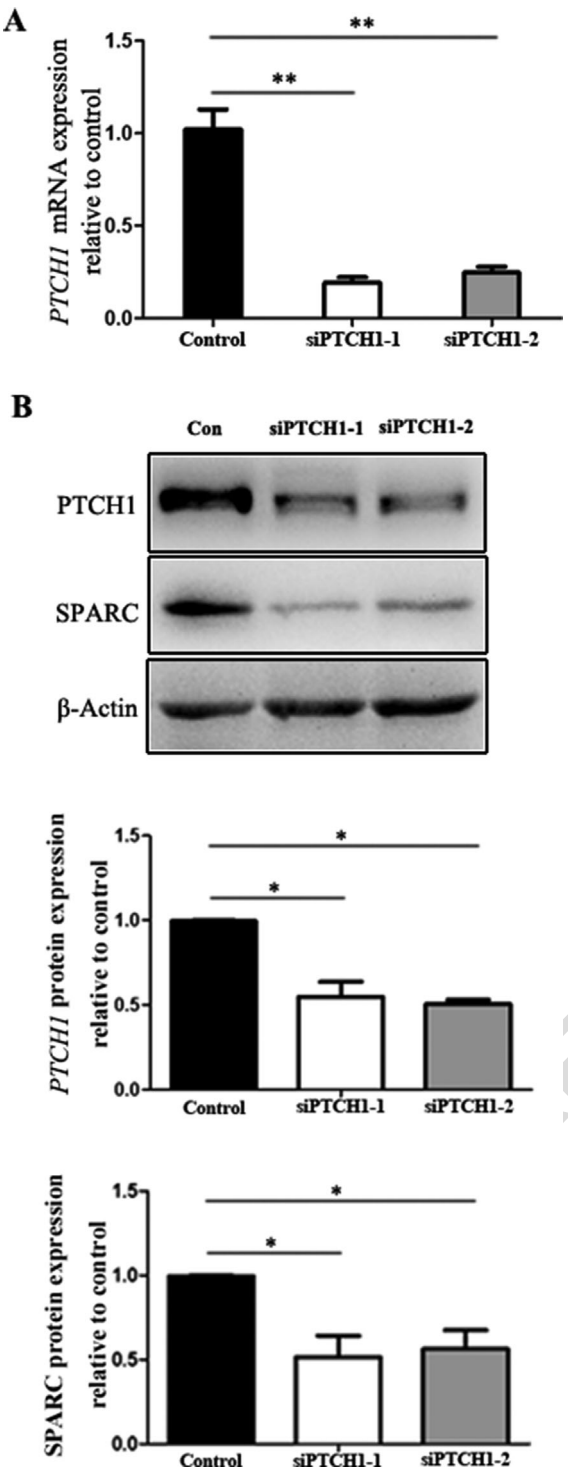

Fig. 4. PTCH1 knockdown causes reduced SPARC expression. (*A*) Knockdown efficiency of PTCH1 in MG63 cells was determined by qPCR at 72 hours. Two siRNAs were both verified to be valid for PTCH1 silencing relative to a control and were tested in three independent experiments. (*B*) The protein expression levels of PTCH1 and SPARC were detected at 72 hours after siRNA transfection using actin as a control. Both siRNAs showed effective silencing. SPARC expression was downregulated after *PTCH1* siRNA transfection compared with the control. The grayscale values of bands were scanned using Image J; error bars are presented as means ± SEM. $^{*}p < 0.05$; $^{**}p < 0.01$ ($n = 3$ technical replicates).

individual of 12 patients with NBCCS harbored the same heterozygous *PTCH1* mutation, implying a germline mutation, whereas none of the non-syndromic stromal cells used as controls were found to harbor *PTCH1* or *SMO* mutations. This indicated that these stromal cells are suitable for the study of the role of heterozygous *PTCH1* mutations in bone metabolism, allowing us to obtain a valuable understanding of the mechanism underlying the development of skeletal abnormalities in NBCCS.

Using LC-MS/MS analysis, we found that SPARC (osteonectin; BM-40) was expressed at 0.6-times lower levels in S-SC cells than in NS-SC cells. SPARC was first detected as a non-collagenous component of bovine and human bone, which bound selectively to both hydroxyapatite and collagen to participate in bone mineral and collagen deposition.[33] The molecular functions and biological characteristics of SPARC have since been elucidated through in vivo and in vitro studies. In adults, SPARC expression is restricted primarily to tissues undergoing renewal and remodeling, such as the ovary and gut, as well as cells of the bone and healing wounds, eg, osteoblasts and fibroblasts.[34–36] During bone remodeling, SPARC binds to collagen I as well as III–V. Then, the SPARC-collagen complex is deposited in the matrix, where it mediates collagen mineralization.[33,37] In the present study, we confirmed lower SPARC expression (~60%) in S-SC cells carrying heterozygous *PTCH1* mutations relative to NS-SC cells used as wild-type controls. The 8 (of 12) samples that harbored protein truncation mutations (NB1, 2, 3, 4, 6, 7, 8, and 10) showed approximately 80% lower SPARC expression. However, in the other 4 cases harboring non-protein truncation mutations, SPARC expression levels were intermediate between those of cells with *PTCH1* truncation mutations and wild-type control cells. These findings were consistent with results of tissue immunochemistry and Western blot analyses. Therefore, the varied expression of SPARC exhibited by individual S-SC cell lines may be attributed to the different types of heterozygous *PTCH1* mutations carried by each line. *PTCH1* protein truncation mutations (observed in 86% of the NBCCS cases) often manifest as PTCH1 haploinsufficiency, as neither the N- nor the C-terminal half of PTCH1 is functional alone.[38,39] *PTCH1* missense mutations have also been reported to result in variable levels of PTCH1 function, with some (Q802L and P1111L) associated with significant retention of activity, some (eg, L346R) causing only modest reduction in activity, and others resulting in substantial loss of function (R280C, G495V, and D499Y).[40,41] Consequently, the missense mutations in the remaining 4 cases (NB5, 9, 11, and 12) may have resulted in the partial retention of function, as a result of which these cases exhibited intermediate levels of PTCH1 activity compared with the wild-type and haploinsufficient lines.

These results, together with those from proteomics analysis, suggest that heterozygous *PTCH1* mutations in syndromic stromal cells, in particular *PTCH1* haploinsufficiency, are implicated in SPARC downregulation. To ascertain the consequences of *PTCH1* loss of function, we introduced siRNAs against *h-PTCH1* into MG63 cells and examined SPARC expression after *PTCH1* silencing in vitro. Our findings indicated that SPARC was downregulated by *PTCH1* silencing. We note that Shigemura and colleagues have shown that *SPARC* may represent a possible target gene of Hh signaling in the prostate, as SPARC upregulation is blocked by cyclopamine in normal prostate fibroblasts but not in cancer-associated prostate fibroblasts.[42] Therefore, we suggest that SPARC may be regulated by the Hh signaling pathway in human marrow-like stromal cells as well.

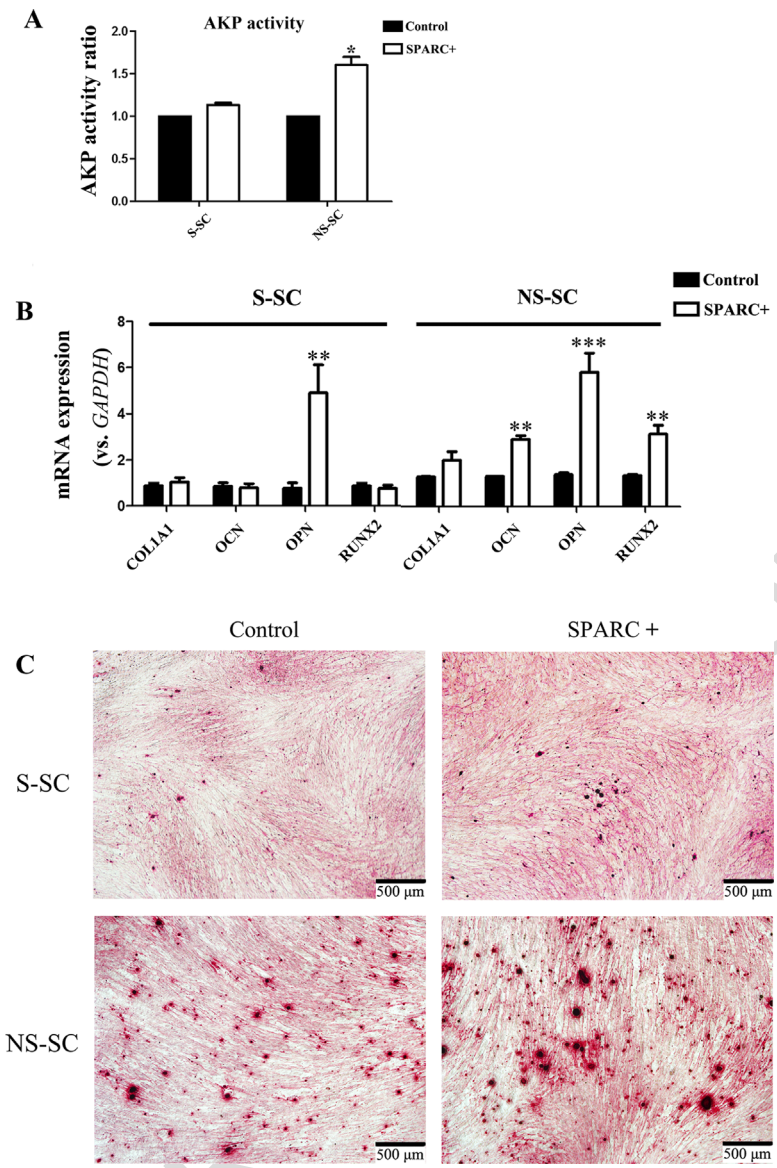

Fig. 5. Exogenous SPARC promoted osteogenic differentiation in syndromic and non-syndromic stromal cells. (*A*) AKP activity was detected 1 week after induction initiation; $^{*}p < 0.05$ ($n = 6$). S-SCs showed no significant difference regardless of SPARC stimulation. NS-SCs showed enhanced AKP activity compared with controls. (*B*) mRNA expression of osteogenesis-related genes were analyzed by real-time qPCR 2 weeks after induction; error bars are presented as means ± SEM. $^{*}p < 0.05$; $^{**}p < 0.01$; $^{***}p < 0.001$ ($n = 6$). (*C*) Alizarin red staining was performed at 3 weeks. Samples stimulated by ectogenous expression of SPARC protein exhibited stronger and greater numbers of calcium nodules than the corresponding controls. S-SCs and NS-SCs showed similar trends after ectogenous SPARC induction ($n = 6$).

We additionally tested whether exogenous SPARC promotes osteogenesis in S-SC and NS-SC cells. Exogenous SPARC added to osteogenesis induction medium elicited enhanced differentiation associated with increased calcium nodule formation and AKP activity in NS-SC cells, whereas S-SC cells showed mildly increased calcium nodule formation. However, the differential protein expression profile indicated that other ossification-associated proteins in addition to SPARC, such as collagen alpha-1 and HSPG2, were downregulated in S-SC cells. Because SPARC has been reported to specifically bind collagen I and regulate its mineralization,[43] the decreased osteogenesis of S-SC cells may result from the corresponding downregulation of COL1A1 expression. The PTCH1 functional deficit in S-SC cells may also account for their different response to SPARC stimulation.

Osteonectin/SPARC, which is one of the most abundant non-collagenous extracellular matrix proteins in bone, plays a major role in regulating collagen fiber assembly and promoting osteoblast differentiation.[44] Several groups have reported that SPARC-null and SPARC-haploinsufficient mice exhibit low-turnover osteopenia that increases with age, showing reduced numbers of osteoblasts and osteoclasts as a result of negative bone balance; these findings support that SPARC contributes to normal bone formation.[45,46] Similarly, mesenchymal stem cells isolated from patients with osteoporosis exhibit SPARC downregulation, which is also frequently found in

A

Person	Sex	Age	Height (cm)	Weight (kg)	Bone mineral density T/Z score: Lumber spine (L1-L4)	Bone mineral density T/Z score: Femoral neck	BMD (g/cm2)	BMI
NB 13	Male	16	187	72	-0.1	-1	0.909	20.59
NB 14	Male	16	176	70	0	-0.8	0.96	22.60
NB 15	Male	16	175	70	2	-0.1	1.017	22.86
NB 16	Male	18	171	52	-2.3	-2.1	0.715	17.78
NB 17	Male	27	195	125	-0.6	0.5	1.116	32.87
NB 18	Male	32	183	83	-0.5	-0.9	0.898	24.78
NB 19	Male	34	178	90	-0.5	-0.8	0.94	28.41
NB 20	Male	39	165	68	-1.4	-1.1	0.774	24.98
NB 21	Male	39	181	90	0	0.3	1.081	27.47
NB 22	Male	46	167	75	1.8	-0.5	1.027	26.89
NB 23	Male	52	175	86	-0.1	-1.9	0.686	28.08
NB 24	Male	60	177	78	-0.2	-1.3	0.872	24.90

B

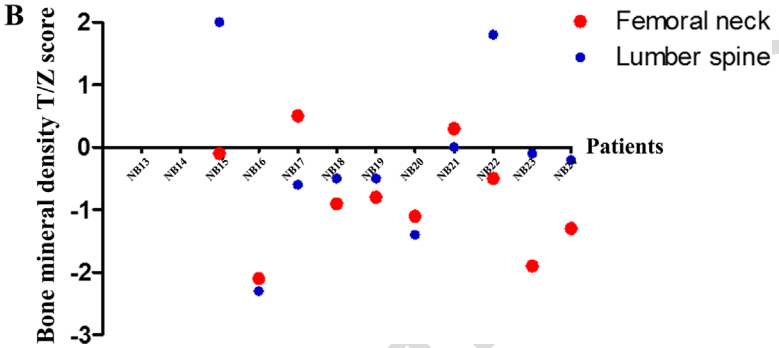

Fig. 6. Bone mineral density of patients with NBCCS. (*A*) Detailed bone mineral density values for 12 patients with NBCCS are listed. (*B*) *T*-scores are shown as a scatter diagram ($n = 12$).

men with idiopathic osteoporosis.[44,47] We, therefore, wondered whether downregulation of SPARC in S-SC cells impacts bone mass in patients with NBCCS. To investigate this hypothesis, we recruited 12 patients diagnosed with NBCCS for BMD analysis, 4 of which were additionally diagnosed with osteopenia according to WHO standards. The others exhibited a comparatively low level of BMD compared with age group standards. The BMD tests suggested that, in addition to bone abnormalities, patients with NBCCS may additionally exhibit lower BMD and be prone to bone mass loss, thus showing an increased risk of fractures. Considering the relatively lower level of SPARC expression associated with *PTCH1* truncation mutations, patients with NBCCS who harbor such germline mutations may be predisposed to osteopenia. The present findings are expected to be of importance in preventing bone loss in this group.

In summary, we performed proteomics analysis via TMT labeling of stromal cells from syndromic and non-syndromic KCOTs and identified a number of proteins exhibiting significantly differential expression in heterozygous *PTCH1* mutants relative to wild-type cells. Several of these identified proteins are being studied by our group; of these, SPARC was most directly related to ossification, as shown in previous studies. The demonstration of SPARC downregulation in S-SC cells provides novel insights into the relationship between bone abnormalities and germline *PTCH1* heterozygous mutations in patients with NBCCS. Our analyses provide evidence that patients with NBSS who harbor germline *PTCH1* truncation mutations are likely at an increased risk for bone loss. Surgical procedures targeted at syndromic-associated KCOTs may be adjusted appropriately in consideration of the low bone mineral density in the jawbones of such patients.

Disclosures

All authors state that they have no conflicts of interest.

Acknowledgments

The study was supported by grants from the National Natural Science Foundation of China (81030018, 30872900, 81300894) and the Doctoral Fund of the Ministry of Education of China (20120001110043).

The authors thank all the patients and their families for donation of tissue and blood samples and for their continued support of our research. In addition, we acknowledge Guo Chuanbin, Peng Xin, Zhang Jianguo, and Wang Diancan (all surgeons of oral and maxillofacial surgery at the Peking

University School of Stomatology) for tissue collection, Feng Yanrui (fresh specimen bank of central laboratory, Peking University School of Stomatology) for sample collection and transportation, and Du Guohong (radiologist of Peking University Third Hospital) for BMD tests. We are grateful to the Protein Chemistry Facility at the Center for Biomedical Analysis of Tsinghua University for sample analysis, and to Gong Yiyi and Deng Haiteng (School of Life Sciences, Tsinghua University) for providing proteomics technical assistance.

Authors' roles: Study design: LT and CF. Study conduct: HY and ZJianyun. Data collection: ZH, QJ, ZJiemei, and ZL. Data analysis: HY, ZJianyun, and ZH. Data interpretation: LT, CF, HY, ZJianyun, QJ, and ZJiemei. Drafting manuscript: LT and CF. Revising manuscript content: HY and ZJianyun. Approving final version of manuscript: LT, CF, HY, ZJianyun, ZH, QJ, ZJiemei, and ZL. HY takes responsibility for the integrity of the data analysis.

References

1. Anderson DE, Taylor WB, Falls HF, Davidson RT. The nevoid basal cell carcinoma syndrome. Am J Hum Genet. 1967;19:12–22.
2. Gorlin RJ. Nevoid basal cell carcinoma (Gorlin) syndrome. Genet Med. 2004;6:530–659.
3. Epstein EH. Basal cell carcinomas: attack of the hedgehog. Nat Rev Cancer. 2008;8:743–54.
4. Shanley S, Ratcliffe J, Hockey A, et al. Nevoid basal cell carcinoma syndrome: review of 118 affected individuals. Am J Med Genet. 1994;15;50:282–90.
5. Kimonis VE, Mehta SG, Digiovanna JJ, Bale SJ, Pastakia B. Radiological features in 82 patients with nevoid basal cell carcinoma (NBCC or Gorlin) syndrome. Genet Med. 2004;6:495–502.
6. Gailani MR, Bale SJ, Leffell DJ, et al. Developmental defects in Gorlin syndrome related to a putative tumor-suppressor gene on chromosome 9. Cell. 1992;69:111–7.
7. Farndon PA, Del Mastro RG, Evans DG, Kilpatrick MW. Location of the gene for Gorlin syndrome. Lancet. 1992;339:581–2.
8. Hahn H, Wicking C, Zaphiropoulous PG, et al. Mutations of the human homolog of Drosophila patched in the nevoid basal cell carcinoma syndrome. Cell. 1996;85:841–51.
9. Athar M, Li C, Kim AL, Spiegelman VS, Bickers DR. Sonic Hedgehog signaling in basal cell nevus syndrome. Cancer Res. 2014;74: 4967–75.
10. Caro I, Low JA. The role of the hedgehog signaling pathway in the development of basal cell carcinoma and opportunities for treatment. Clin Cancer Res. 2010;16:3335–9.
11. Gemmill RM, West JD, Boldog F, et al. The hereditary renal cell carcinoma 3;8 translocation fuses FHIT to a patched-related gene, TRC8. Proc Natl Acad Sci U S A. 1998;95:9572–7.
12. Ohgami N, Ko DC, Thomas M, Scott MP, Chang CC, Chang TY. Binding between the Niemann-Pick C1 protein and a photoactivatable cholesterol analog requires a functional sterol-sensing domain. Proc Natl Acad Sci U S A. 2004;101:12473–8.
13. Li TJ, Yuan JW, Gu XM, Sun LS, Zhao HS. PTCH germline mutations in Chinese nevoid basal cell carcinoma syndrome patients. Oral Dis. 2008;14:174–9.
14. Song YL, Zhang WF, Peng B, Wang CN, Wang Q, Bian Z. Germline mutations of the PTCH gene in families with odontogenic keratocysts and nevoid basal cell carcinoma syndrome. Tumour Biol. 2006;27:175–80.
15. Guo YY, Zhang JY, Li XF, Luo HY, Chen F, Li TJ. PTCH1 gene mutations in keratocystic odontogenic tumors: a study of 43 Chinese patients and a systematic review. PLoS One. 2013;8:e77305.
16. Lindström E, Shimokawa T, Toftgård R, Zaphiropoulos PG. PTCH mutations: distribution and analyses. Hum Mutat. 2006;27:215–9.
17. Pan S, Dong Q, Sun LS, Li TJ. Mechanisms of inactivation of PTCH1 gene in nevoid basal cell carcinoma syndrome: modification of the two-hit hypothesis. Clin Cancer Res. 2010;16:442–50.
18. Nagao K, Fujii K, Saito K, et al. Entire PTCH1 deletion is a common event in point mutation-negative cases with nevoid basal cell carcinoma syndrome in Japan. Clin Genet. 2011;79:196–8.
19. Goodrich LV, Milenković L, Higgins KM, Scott MP. Altered neural cell fates and medulloblastoma in mouse Patched mutants. Science. 1997;277:1109–13.
20. Hahn H, Wojnowski L, Zimmer AM, Hall J, Miller G, Zimmer A. Rhabdomyosarcomas and radiation hypersensitivity in a mouse model of Gorlin syndrome. Nat Med. 1998;4:619–22.
21. Aszterbaum M, Epstein J, Oro A, et al. Ultraviolet and ionizing radiation enhance the growth of BCCs and trichoblastomas in patched heterozygous knockout mice. Nat Med. 1999;5:1285–91.
22. Pazzaglia S, Mancuso M, Atkinson MJ, et al. High incidence of medulloblastoma following X-ray irradiation of newborn Ptch1 heterozygous mice. Oncogene. 2002;21:7580–4.
23. Mancuso M, Pazzaglia S, Tanori M, et al. Radiation-induced tumors in Ptch1-deficient mice basal cell carcinoma and its development: insights from radiation-induced tumors in Ptch-deficient mice. Cancer Res. 2004;64:934–41.
24. Ohba S, Kawaguchi H, Kugimiya F, et al. Patched1 haploinsufficiency increases adult bone mass and modulates Gli3 repressor activity. Dev Cell. 2008;14:689–99.
25. Mak KK, Bi Y, Wan C, et al. Hedgehog signaling in mature osteoblasts regulates bone formation and resorption by controlling PTHrP and RANKL expression. Dev Cell. 2008;14:674–88.
26. Plaisant M, Fontaine C, Cousin W, Rochet N, Dani C, Peraldi P. Activation of Hedgehog signaling inhibits osteoblast differentiation of human mesenchymal stem cells. Stem Cells. 2009;27:703–13.
27. Hong YY, Yu FY, Qu JF, Chen F, Li TJ. Fibroblasts regulate variable aggressiveness of syndromic keratocystic and non-syndromic odontogenic tumors. J Dent Res. 2014;93:904–10.
28. Kimonis VE, Goldstein AM, Pastakia B, et al. Clinical manifestations in 105 persons with nevoid basal cell carcinoma syndrome. Am J Med Genet. 1997;69:299–308.
29. Sun LS, Li XF, Li TJ. PTCH1 and SMO gene alterations in keratocystic odontogenic tumors. J Dent Res. 2008;87:575–9.
30. Jin L, Huo Y, Zheng Z, et al. Downregulation of Ras-related protein Rab 5C-dependent endocytosis and glycolysis in cisplatin-resistant ovarian cancer cell lines. Mol Cell Proteomics. 2014;13:3138–51.
31. Looker AC, Orwoll ES, Johnston CC Jr, et al. Prevalence of low femoral bone density in older U.S. adults from NHANES III. J Bone Miner Res. 1997;12:1769–71.
32. Li TJ, Browne RM, Matthews JB. Epithelial cell proliferation in odontogenic keratocysts: a comparative immunocytochemical study of Ki67 in simple, recurrent and basal cell naevus syndrome (BCNS)-associated lesions. J Oral Pathol Med. 1995;24:221–6.
33. Termine JD, Kleinman HK, Whitson SW, Conn KM, McGarvey ML, Martin GR. Osteonectin, a bone-specific protein linking mineral to collagen. Cell. 1981;26:99–105.
34. Brekken RA, Sage EH. SPARC, a matricellular protein: at the crossroads of cell-matrix. Matrix Biol. 2000;19:569–80.
35. Sage H, Vernon RB, Decker J, Funk S, Iruela-Arispe ML. Distribution of the calcium-binding protein SPARC in tissues of embryonic and adult mice. J Histochem Cytochem. 1989;37:819–29.
36. Bradshaw AD, Sage EH. SPARC, a matricellular protein that functions in cellular differentiation and tissue response to injury. J Clin Invest. 2001;107:1049–54.
37. Boskey AL, Moore DJ, Amling M, Canalis E, Delany AM. Infrared analysis of the mineral and matrix in bones of osteonectin-null mice and their wild-type controls. J Bone Miner Res. 2003;18:1005–11.
38. Wicking C, Shanley S, Smyth I, et al. Most germ-line mutations in the nevoid basal cell carcinoma syndrome lead to a premature termination of the PATCHED protein, and no genotype-phenotype correlations are evident. Am J Hum Genet. 1997;60:21–6.
39. Bailey EC, Milenkovic L, Scott MP, Collawn JF, Johnson RL. Several PATCHED1 missense mutations display activity in patched1-deficient fibroblasts. J Biol Chem. 2002;277:33632–40.
40. Bailey EC, Zhou L, Johnson RL. Several human PATCHED1 mutations block protein maturation. Cancer Res. 2003;63:1636–8.

41. Strutt H, Thomas C, Nakano Y, et al. Mutations in the sterol-sensing domain of Patched suggest a role for vesicular trafficking in Smoothened regulation. Curr Biol. 2001;11:608–13.
42. Shigemura K, Huang WC, Li X, et al. Active sonic hedgehog signaling between androgen-independent human prostate cancer cells and normal/benign but not cancer-associated prostate fibroblasts. Prostate. 2011;71:1711–22.
43. Boskey AL, Doty SB, Kudryashov V, Mayer-Kuckuk P, Roy R, Binderman I. Modulation of extracellular matrix protein phosphorylation alters mineralization in differentiating chick limb-bud mesenchymal cell micromass cultures. Bone. 2008;42:1061–71.
44. Dole NS, Kapinas K, Kessler CB, et al. A single nucleotide polymorphism in osteonectin 3′ untranslated region regulates bone volume and is targeted by miR-433. J Bone Miner Res. 2015;30(4):723–32.
45. Machado do Reis L, Kessler CB, Adams DJ, Lorenzo J, Jorgetti V, Delany AM. Accentuated osteoclastic response to parathyroid hormone undermines bone mass acquisition in osteonectin-null mice. Bone. 2008;43:264–73.
46. Delany AM, Amling M, Priemel M, Howe C, Baron R, Canalis E. Osteopenia and decreased bone formation in osteonectin-deficient mice. J Clin Invest. 2000;105(7):915–23.
47. Dalle Carbonare L, Valenti MT, Zanatta M, Donatelli L, Lo Cascio V. Circulating mesenchymal stem cells with abnormal osteogenic differentiation in patients with osteoporosis. Arthritis Rheum. 2009;60:3356–65.

AUTHOR QUERY FORM

JOURNAL: JOURNAL OF BONE AND MINERAL RESEARCH

Article: jbmr2815

Dear Author,

During the copyediting of your paper, the following queries arose. Please respond to these by annotating your proofs with the necessary changes/additions using the E-annotation guidelines attached after the last page of this article.

We recommend that you provide additional clarification of answers to queries by entering your answers on the query sheet, in addition to the text mark-up.

Query No.	Query	Remark
Q1	Please provide the author's degree.	PhD
Q2	Please provide the author's degree.	PhD
Q3	Please confirm that given names (red) and surnames/family names (green) have been identified correctly.	I confirmed.
Q4	Please confirm whether the color figures should be reproduced in color or black and white in the print version. If the color figures must be reproduced in color in the print version, please fill the color charge form immediately and return to Production Editor. Or else, the color figures for your article will appear in color in the online version only.	In black and white form.
Q5	Please provide the manufacturer's city, state if in US, and country.	Grand island, NY, USA
Q6	Please provide the manufacturer's city, state if in US, and country.	Rochford, IL, USA
Q7	Please provide the manufacturer's city, state if in US, and country.	Salt lake city, UT, USA
Q8	Please provide the manufacturer's city, state if in US, and country.	Salt lake city, UT, USA

WILEY

Journal of Bone and Mineral Research • 111 RIVER STREET • HOBOKEN, NJ 07030
E-MAIL: jbmr@wiley.com

PAGE CHARGE FORM

Per JBMR policy, page charges for published manuscripts are $60 per page up to 8 pages and $120 per page for the 9th and all subsequent pages. **Invited material is not subject to page fees.**

Please return this form with your corrected proofs to Production Editor: jbmr@wiley.com

JOURNAL **Journal of Bone and Mineral Research** VOLUME 31 ISSUE

TITLE OF MANUSCRIPT Heterozygous PTCH1 Mutations Impact the Bone Metabolism in Patients With Nevoid Basal Cell Carcinoma Syndrome Likely by Regulating ~~SPARC Expression~~

MS. NO. NO. OF PAGES 16 AUTHOR(S) Yingying Hong, Jianyun Zhang, Heyu Zhang, Xuefen Li, Jiafei Qu, Jiemei Zhai, Feng Chen, Tiejun Li.

Please calculate your page charge based on the number of pages in the enclosed page proofs.

No. of Pages	Charge (US $)	No. of Pages	Charge (US $)
1	**60**	11	**840**
2	**120**	12	**960**
3	**180**	13	**1,080**
4	**240**	14	**1,200**
5	**300**	15	**1,320**
6	**360**	16	**1,440**
7	**420**	17	**1,560**
8	**480**	18	**1,680**
9	**600**	19	**1,800**
10	**720**	20	**1,920**

Article Type *(please check)*: ☑ Original Article/Clinical Trials/Case Report/Clinical Vignette ☐ Perspective/Review/Commentary/Viewpoint**

***Invited material is not subject to page charges.*.**

TOTAL AMOUNT OF ORDER: $ 1,440

BILL TO:

Name Yingying Hong
Institution Peking University School and Hospital of Stomatology
Address 22 Zhongguancun Avenue South, Haidian District,
Beijing, China

Purchase Order No. 2815

Phone 86 10 82195203
Fax 86 10 62173402
E-mail hong_zz@yeah.net

WILEY

Journal of Bone and Mineral Research • 111 RIVER STREET • HOBOKEN, NJ 07030
E-MAIL: jbmr@wiley.com

COLOR CHARGE FORM

Dear Author:

If you have requested color figures for your article to be published in an upcoming issue of the *Journal of Bone and Mineral Research,* kindly fill out and return this form along with your corrected proofs. Please note that **invited material is not subject to color charges**.

Please return this form with your corrected proofs to Production Editor: jbmr@wiley.com

Thank you.

JOURNAL **Journal of Bone and Mineral Research** VOLUME _____ ISSUE _____

TITLE OF MANUSCRIPT _____

MS. NO. _____ NO. OF PAGES_____ AUTHOR(S) _____

No. Color Pages	Color Charges	No. Color Pages	Color Charges
1	**$900**	**5**	**$4500**
2	**$1800**	**6**	**$5400**
3	**$2700**	**7**	**$6300**
4	**$3600**	**8**	**$7200**

Article Type *(please check)*: ☐ Original Article/Clinical Trials/Case Report/Clinical Vignette ☐ Perspective/Review/Commentary/Viewpoint**

Invited material is not subject to page charges.

TOTAL AMOUNT OF ORDER: $_____

BILL TO:

Name _____ **Purchase Order No.** _____

Institution _____ Phone _____

Address _____

_____ Fax _____

_____ E-mail _____